Thermal Masking Across the Human Body: Patterns, Pathways, and Perceptual Boundaries

Haokun Wang
The University of Texas at Dallas
Richardson, TX, USA
haokun.wang@utdallas.edu

Daniel Honrales
The University of Texas at Dallas
Richardson, TX, USA
daniel.honrales@utdallas.edu

Hyunjae Gil
The University of Texas at Dallas
Richardson, TX, USA
DGIST, Daegu, Republic of Korea
hyunjae.gil@dgist.ac.kr

Jin Ryong Kim
The University of Texas at Dallas
Richardson, TX, USA
jin.kim@utdallas.edu

Figure 1: Potential XR applications with thermal interfaces, driven by the thermal masking illusion, on various body parts.

Abstract

Thermal masking, a vibration-induced illusion in which concurrent tactile input induces a vivid thermal sensation at the tactile site, is a promising mechanism for wearable interfaces and extended reality because it can deliver rich thermal feedback with minimal hardware. While prior work has examined this phenomenon on limited body parts, its expression across the full body remains under exploration. We present four studies mapping thermal masking across eight regions: head, face, neck, arms, hands, torso, legs, and feet. Results show that masking strength is location-dependent, producing perceptual patterns that align primarily with somatosensory pathways rather than proximity. On smaller regions such as the fingers, masking was localized, while on larger areas such as the torso and neck, it extended more broadly. Dorsal–ventral and inter-body tests revealed viable pairings and perceptual boundaries. These findings provide the first comprehensive atlas of body-wide thermal masking, advancing understanding and guiding efficient thermal–tactile interface design.

CHI '26, Barcelona, Spain

ACM ISBN 979-8-4007-2278-3/26/04
https://doi.org/10.1145/3772318.3791601

CCS Concepts

• **Human-centered computing → HCI theory, concepts and models**.

Keywords

Thermal masking, neural pathways, perceptual boundary, thermal illusion, full body

ACM Reference Format:
Haokun Wang, Daniel Honrales, Hyunjae Gil, and Jin Ryong Kim. 2026. Thermal Masking Across the Human Body: Patterns, Pathways, and Perceptual Boundaries. In *Proceedings of the 2026 CHI Conference on Human Factors in Computing Systems (CHI '26), April 13–17, 2026, Barcelona, Spain.* ACM, New York, NY, USA, 22 pages. https://doi.org/10.1145/3772318.3791601

1 Introduction

Thermal feedback is a critical dimension of multisensory experience in Extended Reality (XR). While vibrotactile interfaces dominate current XR systems for conveying texture, impact, and motion, the addition of temperature provides a powerful sense of realism and presence. Feeling the warmth of a virtual fire or the chill of holding an ice cube in VR can dramatically enhance immersion. Yet, engineering practical thermal interfaces remains a major challenge. Thermal actuators are often bulky, slow to respond, and power-hungry, making them difficult to integrate into lightweight wearable systems. These constraints limit both the duration of untethered use and the freedom of movement essential for XR interaction, and scaling thermal feedback systems to global body coverage poses high hardware costs and overhead. As such, the current applications of immersive thermal feedback are restricted by interface range and practicality.

A promising alternative lies in exploiting thermal masking—a perceptual illusion in which a vibrotactile stimulus can dominate and relocate thermal sensation, causing users to feel temperature at the tactile site rather than at the physical thermal source. By harnessing this illusion, it becomes possible to render localized and dynamic thermal feedback using only a small number of thermal actuators in combination with distributed tactile ones. This approach could radically reduce hardware cost and complexity while enabling scalable, wearable XR systems. Prior work has demonstrated the potential of such illusions in targeted contexts, such as haptic gloves for object manipulation [41, 46], sleeves for rendering moving temperature profiles [20, 32], and torso-worn arrays for localized cues [35]. However, these explorations have been limited to select body regions, leaving open fundamental questions about how thermal masking operates across the full body.

The core challenge is to uncover the governing principles of thermal masking. Does it depend primarily on neural connectivity, follow somatotopic proximity, or vary with local thermal sensitivity? Are these principles consistent across very different anatomical regions—such as the small, high-sensitivity fingers and face compared to the large, low-sensitivity torso and legs? What are the boundaries of the effect—can masking cross major anatomical divisions between limbs or even extend across the bilateral midline of the body? And, most importantly, how can these principles be translated into practical strategies for actuator placement, enabling efficient and scalable XR thermal interfaces? Answering these questions is essential not only for advancing scientific understanding of somatosensory integration but also for guiding the design of next-generation XR wearables and multisensory applications.

Importantly, uncovering these principles has direct implications for human experience. Efficient thermal rendering can reduce device bulk, improve long-term comfort, and make multisensory XR more accessible for everyday use. Referred thermal sensations can support emotion-rich interactions—such as warmth in social touch—while reducing the need for heavy, skin-contacting actuators. Reliable high-yield body regions may also benefit users with sensory impairments by providing consistent cues for rehabilitation, balance training, or assisted perception. By situating thermal masking within these human-centered concerns, our work aims to bridge perceptual science with meaningful improvements to how people feel, communicate, and interact in multisensory environments.

To address these questions, we conducted the first systematic, full-body investigation of thermal masking. We evaluated masking across eight body regions, spanning from the head to the feet, and then conducted targeted studies of inter-body and opposite-side conditions to probe the boundaries of the phenomenon. This comprehensive approach allowed us to identify optimal stimulation sites, map coverage patterns, and characterize anatomical constraints, providing both local and extended-body principles of thermal masking.

Our work makes three key contributions. First, we provide the first full-body characterization of thermal masking, identifying optimal stimulation sites and mapping coverage patterns across head, hands, torso, legs, and feet. Second, we reveal the mechanisms underlying masking, including its dependence on nerve pathways, somatotopic proximity, thermal sensitivity, and directional asymmetries across body boundaries. Third, we translate these findings into actionable design guidelines for XR thermal interfaces, offering principles for actuator placement, density, and sequencing that enable efficient yet immersive feedback in gloves, suits, and other wearable systems. Together, these contributions advance both scientific understanding and human-centered design, enabling more comfortable, expressive, and accessible multisensory experiences.

2 Related Work

2.1 Thermal Perception and Sensitivity

The capacity to sense temperature is a vital sensory modality, initiated when thermoreceptors within the skin detect deviations from the body's neutral temperature [7, 39, 47]. Warm and cold receptors, located in the dermal and epidermal layers, transduce these stimuli into neural signals transmitted via dedicated spinal pathways to the insular cortex [1, 11]. However, thermal perception is not uniform across the body; a key feature is its asymmetry and regional variation. Humans are generally more sensitive to cooling than to warming, reflecting a higher density of cold receptors, and thermal thresholds differ substantially by body site [7, 23]. Small, distal regions such as the face, hands, and feet exhibit sharper thresholds than proximal regions such as the chest or back. These differences are critical for both thermal comfort modeling and the design of haptic rendering systems, as they introduce diverse constraints on actuator distribution and density [21]. Recent investigations into thermal perception mechanisms have identified illusory phenomenon [42], that may provide pathways toward more lightweight and efficient design solutions.

2.2 Thermal Masking and Illusions

Thermal masking is a perceptual illusion in which a vibrotactile stimulus can override the location of a thermal input, causing the temperature to be felt at the tactile site rather than at its physical source [42]. This relocation of thermal sensation makes masking particularly relevant for XR: it allows designers to evoke localized thermal feedback using only a small number of thermal actuators combined with widely available tactile ones, reducing hardware cost, power consumption, and bulk [31, 32, 41]. Masking is part of a broader set of thermal illusions that reveal the malleability of temperature perception. A closely related effect is thermal referral, where a thermal sensation is perceived at a site adjacent to—but not directly stimulated by—the source [3, 13, 17]. Unlike referral, which typically requires spatially distributed thermal inputs, masking emphasizes cross-modal dominance, with touch dictating the perceived location of heat or cold.

Other illusions further illustrate this flexibility, such as the thermal grill illusion, where alternating warm and cool inputs induce a painful burning sensation [5], or thermal saltation, where discrete thermal pulses are perceived as continuous thermal motion [40]. While these effects demonstrate the brain's integrative processing of thermal cues, thermal masking stands out as being directly applicable to XR: it enables scalable, efficient thermal interfaces that can extend realism and presence without demanding dense arrays of thermal hardware. For example, thermal masking has been used in gloves simulating object manipulation with strategic thermal actuator placement to avoid interference with hand manipulation [41, 46], in sleeves creating flowing thermal motion through stationary thermal actuators with integration of dynamic thermal and tactile illusions [20, 32], and in torso-worn arrays for localized cues where the thermal actuator was placed along the spine to induce illusionary thermal sensation on lateral axes [35]. Insights drawn from these works reveal great potential for human-centered design, providing sensory-driven approaches to engineering rich, efficient, and expressive thermal experiences without reducing user comfort and convenience.

2.3 Wearable Thermal Interfaces and Thermal Applications

The pursuit of thermal feedback for immersive digital experiences has led to a growing body of work on wearable interfaces. These systems deliver thermal cues via conduction, convection, or radiation. Conduction-based devices remain the most common. Peltier (thermoelectric) elements provide relatively fast heating and cooling and can be scaled to different form factors, from ear-worn [25], facial [28], and chest-worn displays [8], to wrist [27], finger [24, 48], and foot interfaces [9, 22]. Liquid circulation systems represent another conductive approach, delivering temperature through water pumped in flexible tubing to cover large or irregular surfaces [14, 15]. Non-contact solutions based on convection or radiation offer seamless integration but are limited by effective range and calibration requirements [18, 33, 43].

Leveraging these technologies, researchers have built diverse prototypes: fingertip modules [30, 48], wristbands [27], face-integrated systems with HMDs [28, 44], and full-body wearables. Other investigation have exploited illusions to create moving thermal sensations [32], to simulate pain [12], or to blend thermal and tactile feedback for realism. Expanding the engineering benefits to a grander perspective, work in thermal interfaces points towards more profound and expressive sensory experiences in everyday life. For example, integrated thermal feedback can convey affective and emotional signals [45], facilitate deeper embodiment and relation in XR social interactions [26], and create immersive interactions for meditation and rehabilitation [34]. However, such ideas remain isolated and experimental without practical rendering techniques to consolidate their applications into a unified implementation. To realize highly expressive interfaces of wide coverage with minimal cost and encumbrance, investigation of human sensory perception and integration across the full human body is critical [19, 36]. Ultimately, these pursuits collectively point to the potential of perceptual illusions—especially thermal masking—as compact and energy-efficient approaches to building scalable thermal XR interfaces that enrich human-centered experiences while preserving dexterity and agency.

3 System Setup

To investigate body-wide thermal masking, we developed a custom experimental system capable of delivering precisely controlled thermal and tactile stimuli to multiple body regions. The system was designed with three goals: (1) to provide repeatable, safe, and calibrated thermal–tactile stimulation, (2) to accommodate the wide variation in surface curvature, sensitivity, and available area across different body parts, and (3) to enable modular attachment so that the same apparatus could be applied consistently from the face and fingers to the torso and legs. The setup combines Peltier-based thermal modules with linear resonant actuator (LRA) tactile modules, built in small and large configurations depending on the target region. A closed-loop control system ensured precise temperature regulation, while safety protocols and calibration procedures guaranteed consistent delivery across participants and trials.

3.1 Design Goals and Configuration

The system was designed to deliver controlled and repeatable thermal and tactile stimuli across diverse body regions. Stimuli consisted of a +3°C increase above baseline skin temperature and 1 g RMS vibration. Body regions were tested under realistic usage conditions, acknowledging that some areas (e.g., hands, face) are typically exposed, whereas others (e.g., torso, legs) are commonly covered by clothing. To accommodate large differences in surface curvature, garment coverage, and actuator requirements, we developed two modular setups (see Fig. 2):

- **Small setup:** Designed for compact or highly curved regions such as face, head, neck, fingers, palms, and feet. Large actuators would be impractical in these areas and would not reflect realistic wearable designs (e.g., gloves, face-mounted interfaces).
- **Large setup:** Designed for broader and flatter regions such as the torso, arms, and legs. These areas benefit from larger thermal surfaces and require stronger vibration output, particularly through clothing on torso, aligning with how these regions are typically stimulated in wearable XR systems.

A potential concern is that these different sizes could confound the observed masking patterns. To address this, we conducted pilot comparisons in overlapping regions and found that masking strength and spatial spread were consistent across module sizes.

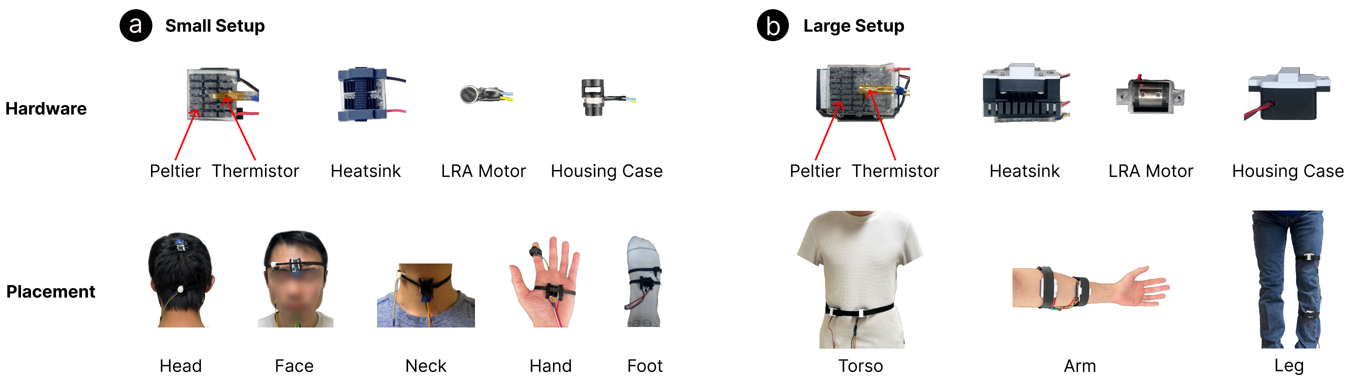

Figure 2: Experiment apparatus of the study for (a) small and (b) large setup, with hardware components and apparatus placement relative to each body region.

This confirms that the results reflect body-region properties rather than hardware differences.

Another concern is the temporal simultaneity of thermal and vibrotactile inputs, given the much slower rise time of thermal stimuli. Pilot testing showed that thermal masking illusion remains robust even when the thermal percept reaches threshold up to 2 s after the vibrotactile onset, consistent with the slow temporal integration of warm perception [32]. In our experiments, the command onsets for thermal and vibrotactile stimuli were programmatically synchronized, producing hardware trigger offsets <10 ms. Vibrotactile stimulus reached full intensity within <0.1 s, while thermal stimuli reached perceptual threshold within <1 s, well within the empirically validated tolerance window.

3.2 Thermal Stimulation Module

Thermal stimulation was delivered using Peltier-based modules optimized for controlled heating and efficient cooling.

- **Small module:** A Peltier element (26 ×26 mm, 2.3 mm thick; FTED S017A026026), mounted in a 3D printed housing with an aluminum heat sink.
- **Large module:** A Peltier element (30 ×40 mm, 2.3 mm thick; FTED S043A030040), housed similarly but paired with both an aluminum heat sink and a 5V DC fan to manage the higher thermal load.

The sizes of the small and large thermal actuators were selected based on practical considerations for wearable XR devices and the anatomical constraints of each body region. The 26 × 26 mm module was chosen for highly curved or compact surfaces—such as the fingers, palm, face, neck, and the dorsal/plantar regions of the feet—where a smaller footprint ensures stable contact and aligns with glove-, face-, and shoe-based thermal interfaces. By contrast, the larger 30 × 40 mm module was used for broader, flatter areas including the torso, arms, and legs, where increased contact area supports more stable heat transfer and provides a thermal mass representative of vest- or suit- style XR systems. These size selections reflect both ergonomic considerations and realistic form factors for future full-body XR thermal wearables.

In both setups, a thin-film thermistor (TEWA TT6-100KC3L-5-AUR) provided real-time temperature feedback at 1 kHz sample rate via an Arduino Uno. A programmable DC power supply (Korad KD6005P) regulated actuator voltage under closed-loop PID control, maintaining a +3 °C offset relative to baseline skin temperature during each 5 s trial. The average rise time to reach the target skin temperature was less than 1 s. A cooling fan and heatsink were incorporated for the large module to accelerate cooldown; the fan activated immediately after each trial and deactivated once the module temperature returned to baseline. The small module omitted the fan to preserve flexibility on highly curved surfaces. For both modules, surface temperature returned to baseline within less than 20 seconds.

Importantly, this natural cooldown time was faster than the scheduled 30-second inter-trial interval, and the modules were fully removed from the skin between trials. Because removal prevents residual conductive heating, this protocol provided a conservative buffer against thermal adaptation or skin fatigue. Analyses of early versus late trials within each study showed no drift in masking occurrence rates, confirming that thermal adaptation did not confound the perceptual results.

To ensure accurate thermal delivery, a calibration procedure was conducted for each body region. For direct skin contact, the thermistor was affixed to the Peltier surface, and an average actuator heating rate of 6°C/s reliably produced the required +3°C skin increase. For cloth-covered regions, thermistors were temporarily placed on both the actuator surface and the skin to derive the overdrive needed to achieve the same +3°C offset through fabric. For consistency, calibration was performed at an accessible location on the corresponding region (e.g., upper back for torso). Due to the increased thermal resistance of clothing, higher heating rates were required: 9°C/s for a thin 0.5 mm polyester shirt and 15°C/s for 1 mm denim. These calibrated heating profiles ensured that the delivered skin temperature change was consistent across all body regions and garment conditions.

3.3 Tactile Stimulation Module

Tactile stimulation was delivered using linear resonant actuators (LRAs) operated at their respective resonant frequencies to ensure efficient and perceptually salient vibration.

- **Small module:** LRA motor (10 mm diameter, 3 mm thick; JYLRA1040ZF, JIEYI Co.) driven at resonant frequency of 180 Hz.
- **Large module:** LRA motor (22 × 30 mm, VG2230001H, Vybronics) driven at resonant frequency of 70 Hz.

Both actuators were powered by a Class-D audio amplifier (PAM8610, HiLetgo), calibrated to deliver a unified 1 g RMS acceleration, and mounted in custom 3D-printed housings that ensured stable coupling across body regions. Because each LRA was driven at its resonant frequency (180 Hz for the small module and 70 Hz for the large module), the resulting vibrations fall within the sensitivity range of cutaneous mechanoreceptors—particularly Pacinian corpuscles—supporting reliable detection across the anatomical sites studied [37]. Both LRAs exhibited short response times (<0.1 s), enabling low-latency vibrotactile delivery synchronized with the thermal stimulus.

3.4 Attachment, Safety, and Calibration Protocols

All modules were enclosed in 3D-printed housings and secured to the body using adjustable Velcro straps. Placement was standardized using anatomical landmarks and verified with a tape measure to ensure repeatability across participants. To minimize variability, housing end-effectors (10 mm for small modules, 20 mm for large modules) ensured consistent contact area with the skin.

Safety protocols were implemented to protect participants and maintain stimulus fidelity. Upon arrival, participants rested for 10 minutes to stabilize skin temperature. Modules were removed between trials to allow recovery, and a 30-second break was enforced every 30 trials to prevent fatigue. The control software included an automatic cutoff to prevent overheating of the thermal actuators. For tactile actuators, the PLA protrusions minimized thermal transfer from the motors, keeping self-heating below 0.3 °C during a 5-second activation.

Calibration procedures were conducted prior to all experiments to ensure consistent stimulus delivery across conditions. Vibration output was verified at 1 g RMS acceleration using an accelerometer (Kistler 8794A), and thermal output was calibrated to +3 °C above baseline using a thin-film thermistor (TEWA TT6-100KC3L-5-AUR). The same thermistor was used for real-time monitoring during trials (as described in Section 3.2), ensuring continuity between calibration and closed-loop operation. Signals were logged with a data acquisition system (cDAQ 9171, NI) to confirm stability and reproducibility. The detailed attachment on all body parts can be seen in Figure 2.

4 Study 1: Head, Face, and Neck

4.1 Motivation

The head, face, and neck are especially relevant for wearable and XR systems, as these regions are in direct contact with devices such as head-mounted displays and neck-worn accessories. The complex cranial innervation of these areas may influence how thermal illusions are perceived, making them important for understanding how thermal masking can be applied in practice. This study aimed to identify effective locations and perceptual ranges for thermal masking, examining whether masking strength and spread vary across small, curved regions such as the face compared to larger surfaces such as the neck. We systematically evaluated three anatomical subregions: head, face, and neck.

4.2 Participants

Twelve participants (2 female and 10 males; $M = 27.4$, $SD = 3.4$, $Min = 21$, $Max = 32$; all right-handed) were recruited from the university community through online advertisements. Each received a $10 gift card as compensation. Participants were screened via questionnaire to exclude those with neuropathy or skin injuries. The study protocol was approved by the Institutional Review Board, and written informed consent was obtained from all participants.

4.3 Study Design

This study used a within-subjects design to map the perceptual characteristics of thermal masking across the head, face, and neck. The independent variables were the location of the thermal stimulus and the location of the concurrent vibrotactile stimulus.

Because these regions involve compact and highly curved surfaces, all tests used the small setup (see Section 3), consisting of a 26 × 26 mm Peltier thermal module and a 10 mm LRA mounted in a 3D-printed housing. Stimulus sites were selected to reflect both anatomical and application-driven considerations. Specifically, site selection accounted for local surface curvature, proximity to major cranial and cervical nerve branches, and the practical constraints of achieving stable contact with a compact thermal module. We additionally aligned the site layout with regions commonly engaged by XR hardware: facial positions correspond to typical HMD contact points (cheek pads, brow strap, temple anchors), while head and neck locations match areas where headbands, straps, and emerging thermal-tactile accessories interact with the skin. Final site counts and spacing were refined through pilot tests to ensure safe mounting, stable contact, and clear perceptual discriminability of masking across positions. Detailed placement configurations for each region are provided below.

- **Head Region:** Seven positions were tested on the scalp (see Figure 3 (a)). A single thermal stimulus was applied at the vertex, corresponding to the overhead strap location of many HMDs. Six vibrotactile sites were distributed along sagittal and coronal planes between the vertex and ear, covering typical side-strap regions. This produced 6 unique conditions.
- **Face Region:** Fourteen positions were tested across the face (see Figure 3 (b)). Six thermal sites were selected at key HMD contact points, including the supraorbital ridge (eyebrow), zygomatic arches (cheeks), and mentum (chin). Each thermal site was paired with 13 vibrotactile sites spanning trigeminal dermatomes, producing 78 unique conditions.
- **Neck Region:** Twelve positions were tested on the neck (see Figure 3 (c)). Two thermal sites were placed at the anterior and posterior midlines, corresponding to neck support points. Each was paired with 11 vibrotactile sites distributed across ventral, dorsal, and occipital regions, producing 22 unique conditions.

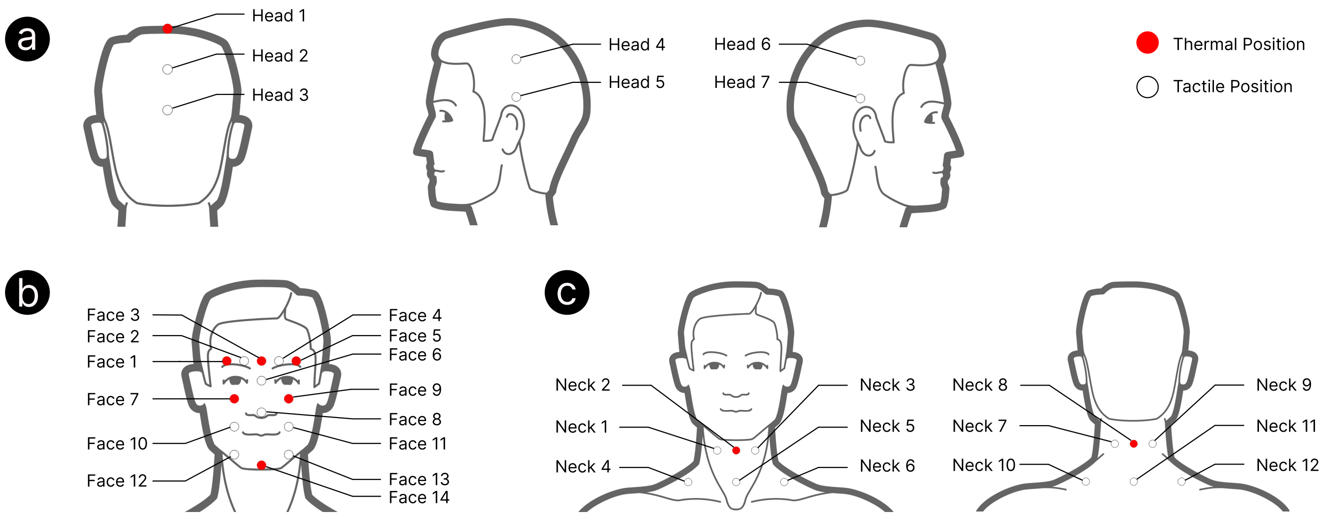

Figure 3: Tested positions for (a) Head, (b) Face, and (c) Neck. The red circle indicates the positions for thermal stimuli. The black circle indicates the positions for tactile stimuli other than the thermal position.

In total, the design included 106 unique conditions. Each participant completed two repetitions of all trials, with order randomized to minimize order effects. To reduce fatigue, the experiment was divided into two sessions conducted on separate days, yielding 212 trials per participant.

Measures. The primary measure was the occurrence rate of thermal masking, defined as the proportion of trials in which participants reported a thermal sensation at the tactile site. A secondary measure was the extent and distribution of drawn thermal areas, capturing the perceived spread.

4.4 Procedure

Upon arrival, participants provided informed consent and rested for 10 minutes to stabilize skin temperature, measured by a thin-film thermistor. Actuators were positioned at the designated locations according to anatomical landmarks.

During each trial, participants closed their eyes while concurrent thermal (+3 °C above baseline, 5 s) and vibrotactile (1 g RMS) stimuli were delivered. After each stimulus, participants reported whether they experienced a thermal sensation at the tactile site. When present, they used a mouse to draw the perceived thermal area on a digital diagram of the stimulated body part (PC: Alienware R12). Modules were removed between trials to allow skin temperature to return to baseline. A 30-second break was enforced every 30 trials. Each session lasted approximately 1.5 hours.

4.5 Results

Overall Observations. Thermal masking was typically localized around the thermal cue, with participants often reporting sensations confined to the immediate stimulation site (see Figure 4-6). In some cases, however, the masking extended well beyond the point of contact, producing percepts that followed neural pathways rather than simple proximity (see Figure 6).

To ensure sufficient statistical power for within-subject comparisons, we conducted an a priori power analysis using G*Power (F-tests; repeated measures ANOVA). Assuming a large effect size (f=0.40) a target power of 0.80, α=0.05, and a moderate correlation among repeated measures (r=0.5), the analysis indicated that 12 participants were required for our primary conditions involving six repeated measurements (head regions). A subsequent post-hoc analysis confirmed that N=12 remained adequate for the more complex conditions involving thirteen repeated measurements (face regions) and eleven repeated measurements (neck regions). To ensure the reliability of the experimental measurements, we performed an analysis using the Intraclass Correlation Coefficient (two-way random effects, average measures). The results yielded an ICC(2,k) of 0.69, indicating moderate reliability. We maintained the protocol of two repetitions per condition to balance measurement stability with total experiment duration. Based on these results, we adopted N=12 for each body region. While this sample size is consistent with prior psychophysical work [3] and statistically powered for within-subject contrasts, we acknowledge that generalizing to population-level thermal-masking norms will benefit from larger-scale follow-up studies.

Head. On the head, masking was confined and selective. Most participants reported thermal sensations closely tied to the tactile cue, with only limited spread across adjacent sites. Referral tended to align along the coronal plane, where masking extended slightly further than along the sagittal axis (see Figure 4). This suggests that only a subset of scalp sites are optimal for eliciting strong illusions.

Statistical analysis confirmed these patterns: A one-way RM-ANOVA revealed significant effects of tactile position ($F(5, 55) = 17.22$, $p < 0.01$, $\eta_p^2 = 0.47$). Post-hoc comparisons identified *Head 2, 4,* and *6* as the most effective positions ($p < 0.01$). These findings reinforce the observation that scalp masking is limited in range and stronger along the coronal than the sagittal plane.

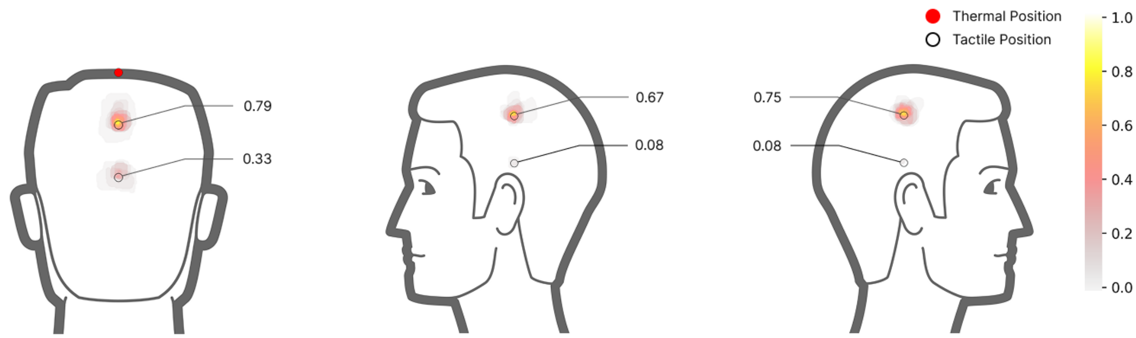

Figure 4: Distribution of perceived thermal illusion area under Head conditions with occurrence rate noted for each tactile position.

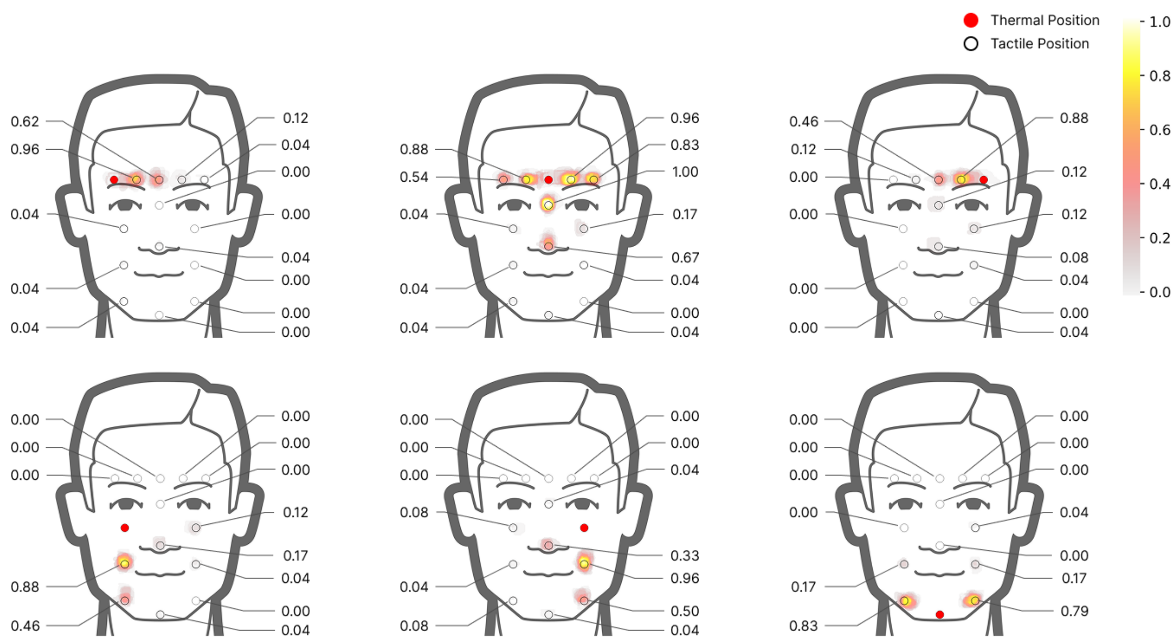

Figure 5: Distribution of perceived thermal illusion area under Face conditions with occurrence rate noted for each tactile position.

Face. The face showed broader and more dispersed masking than the head, with central sites often producing referral across multiple neighboring regions. For example, stimulation around the supraorbital ridge (Face 3) resulted in widespread referral to adjacent cheek and chin areas, highlighting the face's potential to support broad thermal illusions. At the same time, certain sites produced highly localized effects—for instance, Face 7 generated referral almost exclusively to Face 10. This suggests that while the face can generate broad spread, the effect depends strongly on the chosen thermal site.

These patterns were reflected in statistical tests: a two-way RM-ANOVA revealed significant main effects of thermal site ($F(5, 55) = 42.73$, $p < 0.01$, $\eta_p^2 = 0.29$), tactile site ($F(13, 143) = 15.37$, $p < 0.01$, $\eta_p^2 = 0.19$), and their interaction ($F(65, 715) = 42.01$, $p < 0.01$, $\eta_p^2 = 0.69$). Post-hoc analysis confirmed Face 3 as the most effective thermal site, producing robust masking to Face 2, 4, 5, and 6. Face 3 also produced the most dispersed perceived thermal area, in contrast to localized positions such as Face 7, where masking was limited to Face 10 (see Figure 5).

Neck. The neck exhibited broad and selective patterns of masking, often spreading across distant sites rather than remaining confined to local areas. Participants frequently reported sensations extending toward the sides and back of the neck, making this region the most widely dispersed compared to the head and face (see Figure 6). A consistent lateral preference was observed: anterior stimulation at Neck 2 was most effective at lateral sites (Neck 1, 3, 7, 9), while medial sites such as Neck 8 were weaker. Similarly,

Figure 6: Distribution of perceived thermal illusion area under Neck conditions with occurrence rate noted for each tactile position.

posterior stimulation at Neck 8 produced strong referral to lateral positions (Neck 7, 9, 10) but weaker masking at the closer medial site Neck 11.

Statistical results supported these observations: a two-way RM-ANOVA with GG correction revealed significant effects of tactile position ($F(11, 121) = 12.70$, $p < 0.01$, $\eta_p^2 = 0.24$) and significant interaction with thermal site ($F(11, 121) = 11.98$, $p < 0.01$, $\eta_p^2 = 0.15$). For anterior stimulation (Neck 2), masking was strongest at adjacent sites (Neck 1, 3) but also extended to distant lateral sites (Neck 7, 9) at 65%. For posterior stimulation (Neck 8), lateral sites (Neck 7, 9) showed the highest occurrence (>90%), with additional spread to more distant sites (Neck 3, 10) above 65%. Post-hoc comparisons confirmed higher occurrence rates for lateral positions, reinforcing the observed lateral spread and highlighting the neck as one of the most dispersed regions.

Cross-region comparison. Across regions, clear differences emerged in the spread of thermal masking. On the head, effects were the most localized, with strong masking restricted to a few coronal sites and minimal propagation. The face exhibited broader masking, particularly from central sites such as Face 3, but the spread was largely clustered within adjacent facial areas. By contrast, the neck showed the most dispersed referral patterns, with sensations extending across distant sites and a consistent preference for lateral pathways. This makes the neck unique in supporting both near and far referral, whereas the head and face were relatively constrained.

Additional observations. Several consistent patterns also emerged across regions. First, the degree of spread followed a systematic progression: masking on the head was tightly localized, the face produced broader but clustered spread, and the neck was the most dispersed. Second, lateral–medial asymmetries were robust, with lateral sites generally producing stronger masking than medial ones (e.g., Neck 7 and 9 > Neck 11), and coronal positions outperforming sagittal ones on the head. Together, these findings highlight that referral patterns are constrained more by innervation boundaries than by geometric distance, underscoring the role of nerve pathways in shaping thermal masking illusions.

4.6 Discussion

The results from Study 1 reveal distinct patterns of thermal masking across the head, face, and neck. On the head, referral was highly localized, with only a few coronal sites producing reliable effects. The face supported broader masking, especially from central supraorbital sites such as Face 3, but the spread remained clustered within adjacent regions. In contrast, the neck exhibited the most dispersed patterns, with referral extending to both nearby and distant sites and showing a consistent lateral preference. This progression—from localized (head) to broad but clustered (face) to highly dispersed (neck)—suggests that different body regions afford different ranges of thermal referral.

Masking patterns aligned more closely with innervation boundaries than with geometric distance. On the face, for instance, stimulation at a supraorbital site spread strongly to adjacent regions innervated by the ophthalmic branch (V1) but weakly to a closer maxillary site (V2). On the neck, lateral supraclavicular pathways consistently produced stronger referral than nearby medial cervical sites, even when physically closer. In some cases, distant lateral sites outperformed nearer medial ones, highlighting a systematic lateral preference. These findings suggest that thermal masking propagates preferentially along functional sensory branches, providing a mechanistic explanation for why spread varies so strongly across regions.

Design Implications. For XR interfaces targeting the head, actuator placement should focus on a small number of optimal scalp sites along the coronal plane, where masking is most effective and reliable. On the face, central placements near the supraorbital ridge are particularly valuable, as they can induce wide coverage across the cheeks and chin, reducing the number of actuators. On the neck, lateral positions are highly efficient, as they produce both local and far-spreading masking, making them ideal for distributed coverage. Together, these results indicate that carefully chosen sites—rather than dense arrays—can maximize perceptual coverage in head-mounted XR systems such as HMD straps or face cushions.

In Application. The facial regions exhibit substantial potential for thermal interaction. In addition to enabling lifelike sensations—such as wind chill or localized warming—through immersive feedback [28, 31, 44], controlled thermal stimulation applied to cephalic and cervical areas can directly modulate users' thermal comfort [36]. However, due to the high tactile sensitivity of these regions and their susceptibility to encumbrance, interfaces designed for these areas must emphasize minimal intrusiveness and ergonomic integration. Building on the high-efficacy locations identified in this study, the strategic and natural incorporation of thermal masking techniques into existing headgear (see "Thermal HMD" in Figure 18) enables effective thermal expression while maintaining user comfort.

5 Study 2: Hands and Arm

5.1 Motivation

The hands and arms are critical regions for XR interaction, as they are in frequent contact with haptic devices such as controllers, gloves, wristbands, and sleeves. These areas are characterized by the complex distribution of the brachial plexus and high motor precision, which may shape how thermal illusions are induced. This study aimed to characterize thermal masking across the upper limbs, comparing its manifestation on the small, geometrically complex hand versus the larger, relatively flat surface of the arm. We systematically investigated three anatomical regions: the fingers, the hand, and the arm.

5.2 Participants

Twelve individuals (5 females and 7 males; M = 25.9, SD = 3.8, Min = 23, Max = 36; all right-handed) participated in this study, none of whom had taken part in Study 1. Participants underwent the same screening procedure as in the previous study. Recruitment followed the same procedure as in the previous study.

5.3 Study Design

A within-subjects design was used to map the perceptual characteristics of thermal masking across the fingers, hand, and arm. To keep sessions manageable and based on bilateral symmetry, all trials were conducted on the left side of the body. Two setups were used (see Section 3): the small setup for fingers and hand, and the large setup for the arm. Stimulation sites were chosen for their alignment with brachial plexus nerve distributions and their relevance for wearable interface placement. The upper limb presents a complex morphology characterized by both high-curvature surfaces (fingers) and predominantly planar surfaces (arm). To accommodate these geometric differences, we implemented proper modular setup: small modules were applied to the finger and hand regions, while large modules were designated for the arm. Stimulus sites were selected based on both anatomical landmarks and application requirements. Specifically, we targeted the phalanges and dorsal/ventral aspects of the hand to include all major joints. On the arm, we prioritized primary muscle bellies and interaction surfaces. Furthermore, site selection was informed by the affordances of standard XR hardware, ensuring alignment with the interaction zones commonly utilized by haptic gloves and sleeves. The placement of these sites was refined through pilot testing following the same procedure established in previous study. The positions are detailed as follows.

- **Finger region:** The ventral and dorsal sides of the fingers were tested separately. On the ventral side, 14 tactile positions were selected, with 5 also serving as thermal sites (thumb proximal, and middle phalanges of the index, middle, ring, and pinky, see Figure 7 (a)). On the dorsal side, 9 tactile positions were tested, with the same 5 phalanges used for thermal stimulation. This yielded 105 conditions.
- **Hand region:** Five ventral positions were selected (center and four corners of the palm), with the central palm serving as the thermal site (see Figure 7 (b)). Five corresponding dorsal positions were also tested, with the dorsal center as the thermal site. This yielded 8 conditions.
- **Arm region:** Twelve positions were tested across the forearm and upper arm (see Figure 7 (c)). Two ventral sites (center of the forearm and center of the upper arm) served as thermal sites. This yielded 22 conditions.

Measures. Same measurement of the occurrence rate of thermal masking and the distribution of drawn thermal areas were implemented as in Study 1.

5.4 Procedure

The procedure was identical to Study 1. Participants rested to stabilize skin temperature, and trials consisted of simultaneous thermal and tactile stimulation for 5 seconds. The small setup was used for fingers and hand, and the large setup for the arm.

5.5 Results

Overall Observations. The thermal masking effect was generally widespread within the test region (see Figures. 8-11). This was particularly evident on the arm, where the perceived illusion covered the full range (see Figure 11). Interestingly, the results for the fingers showed a more complex pattern, where the perceived area was generally aligned with neural pathways but also regulated by proximity (see Figures. 8-9). Same power analysis was conducted as the previous study to validate the sample size. The reliability result of ICC(2,k) yield a moderate score of 0.68 for 2 repetitions.

Finger. On the ventral side, masking often spread across multiple fingers. For example, stimulation on the middle finger (Finger 17) produced referral across all five fingers. Certain sites showed preferential spread, such as stimulation on the ring finger (Finger 19) producing stronger referral to the pinky (Finger 21–23) than to the middle finger (Finger 15–17) (see Figure 8).

Statistical analysis confirmed these effects: a two-way RM-ANOVA revealed significant main effects of thermal position ($F(4, 44)$ = 15.47, $p < 0.01$, $\eta_p^2 = .10$), tactile position ($F(13, 143) = 9.33$, $p < 0.01$, $\eta_p^2 = .12$), and their interaction ($F(52, 572) = 27.69$, $p < 0.01$, $\eta_p^2 = 0.60$). Post-hoc comparisons revealed significant clusters of referral along adjacent phalanges (e.g., Finger 10; Fingers 12–14; Fingers 15–17).

On the dorsal side, referral was more confined, with significant effects of thermal position ($F(4, 44) = 6.04$, $p < .01$, $\eta_p^2 = .063$), tactile position ($F(8, 88) = 13.15$, $p < .01$, $\eta_p^2 = .16$), and interaction ($F(32, 352) = 27.23$, $p < .01$, $\eta_p^2 = .53$). Post-hoc analysis identified localized clusters, such as Finger 3–4 and Finger 7–9, when stimulated at Finger 2, 4, 6, or 8 (see Figure 9).

Hand. The central palm was the most effective site, producing referral across the entire hand with consistently high occurrence rates (> 75%). Referral was evenly distributed across both ventral and dorsal tactile sites, and the perceived area was substantially larger than the physical stimulus site (see Figure 10). Statistical analysis found no significant effects of thermal or tactile position, consistent with the uniform distribution.

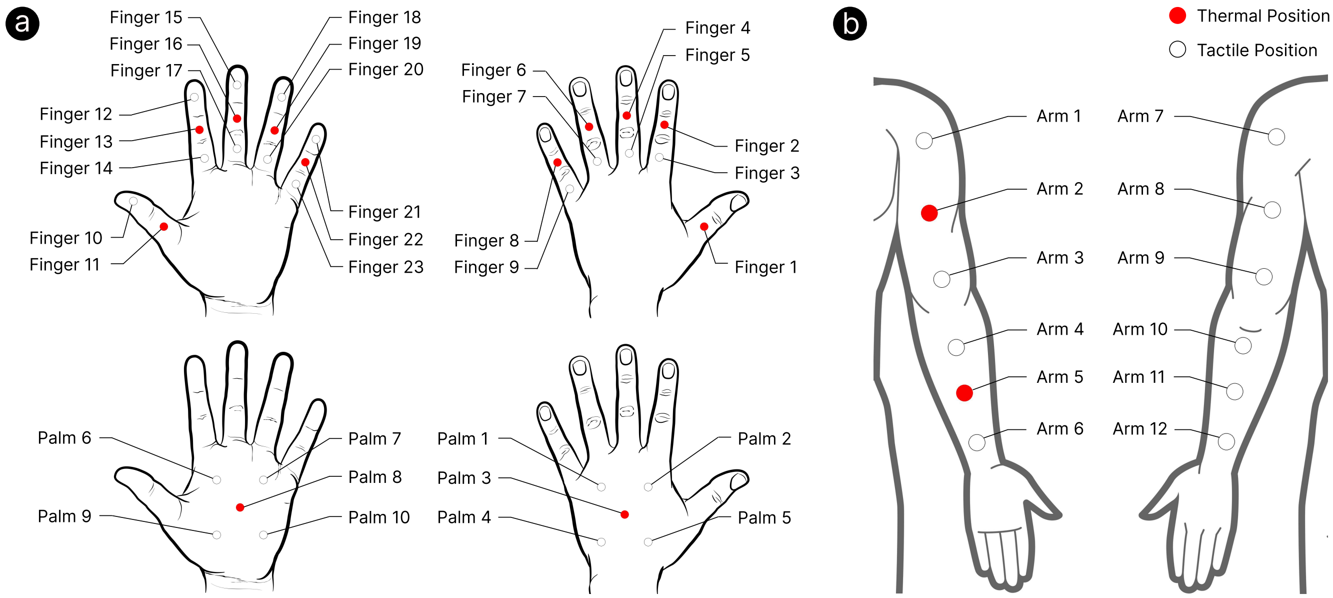

Figure 7: Tested positions for (a) Hands and (b) Arm. The red circle indicates the positions for thermal stimuli. The black circle indicates the positions for tactile stimuli other than the thermal position.

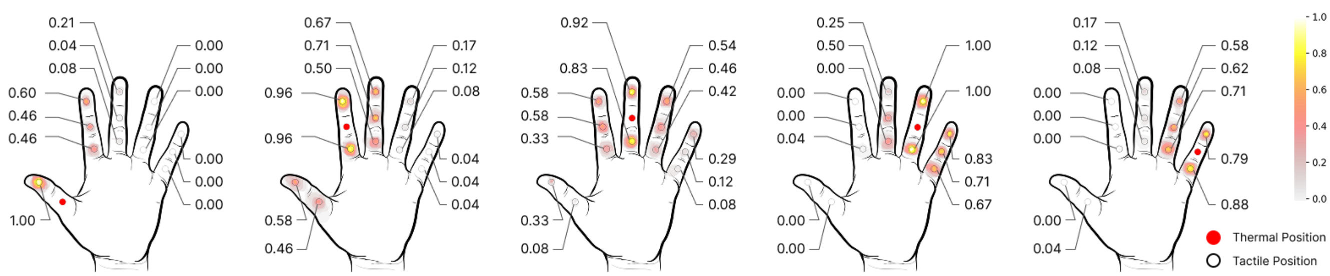

Figure 8: Distribution of perceived thermal illusion of Finger ventral conditions with occurrence rate noted for each tactile position.

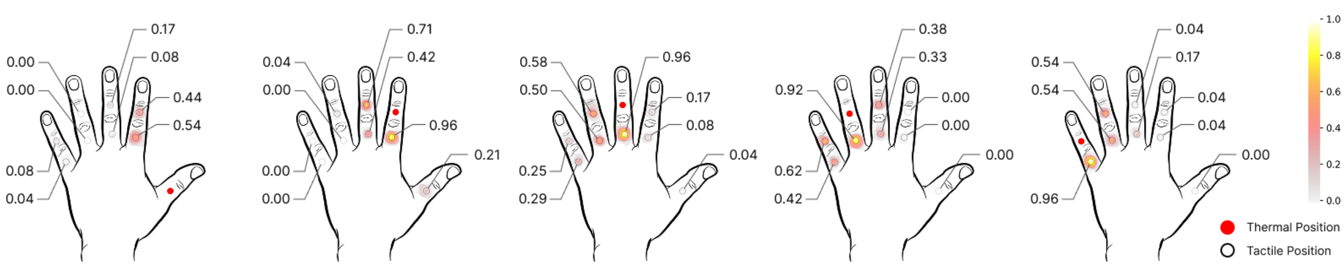

Figure 9: Distribution of perceived thermal illusion of Finger dorsal conditions with occurrence rate noted for each tactile position.

Arm. Referral on the arm was broad, covering both ventral and dorsal surfaces, but strongest effects were concentrated near the stimulation sites (see Figure 11). Central ventral stimulation produced wider spread than more distal sites.

Statistical tests revealed significant effects of thermal site ($F(1, 11) = 21.28$, $p < .01$, $\eta_p^2 = .08$), tactile site ($F(11, 121) = 9.84$, $p < .01$, $\eta_p^2 = .31$), and their interaction ($F(11, 121) = 20.46$, $p < .01$, $\eta_p^2 = .15$). Post-hoc comparisons confirmed higher occurrence rates near the stimulation sites, such as Arm 1 and 3 for stimulation at Arm 2, and Arm 3, 4, and 6 for stimulation at Arm 5.

Cross-region comparison. Distinct spatial profiles emerged across regions. The fingers showed highly localized referral, strongest within adjacent phalanges and on the same finger. The hand displayed uniform referral patterns, with central palm stimulation producing broad coverage across both surfaces. The arm exhibited the most widespread referral, extending dorsally, but effects were still strongest near the thermal site. These differences underscore the heterogeneous nature of somatosensory processing across the upper limb.

5.6 Discussion

The observed thermal illusion patterns were broadly consistent with the neuroanatomy of the brachial plexus (see Figure 12). Effects were strongest when thermal and tactile sites were located within the cutaneous field of the same nerve branch. For example, when thermal stimulation was applied to the ring finger (Finger 19), referral was stronger to the pinky (Finger 22) than to the middle finger (Finger 17, median nerve), even though the latter was physically closer. Cross-nerve referral was generally weaker, although proximity sometimes overrode these boundaries, as seen in the strong referral between the dorsal index (radial nerve) and middle finger (median nerve).

The uniform referral patterns observed on the hand and arm can be interpreted through overlapping dermatomes. Central palm stimulation spanned both C7 and C8, producing broad and consistent illusions across the hand. Similarly, central forearm and upper arm stimulation engaged multiple dermatomes (C5–T1), resulting in widespread referral along the ventral arm. In contrast, more distal or branch-specific sites produced selective illusions, with proximity effects shaping their extent.

Design Implications. For gloves, actuators placed on three key digits—the thumb, middle finger, and pinky—combined with a central palm actuator can achieve broad coverage with relatively few actuators. This configuration leverages both localized and bilateral spread while leaving fingers available for manipulation tasks. For sleeves, placing actuators at the center of the forearm and upper arm efficiently engages multiple dermatomes, creating long-range coverage along the limb without requiring dense actuator arrays. These results provide a blueprint for designing upper-limb haptic devices that maximize perceptual coverage by aligning actuator placement with major nerve fields and areas of natural spread.

In Application. Arguably the most dynamic and interactive regions of the body, the hand and arm hold great potential for immersive experience through sensory enrichment [30, 32, 41, 48]. Inducing thermal masking from the reduced thermal actuator placements found in this study offers the means to increase rendering resolution without hindering dexterity and comfort. Consider feeling the warmth of a handshake or hug without the distracting presence of bulky hardware, or tangibly exploring the thermal profile of an object surface with the complete flexion range of the hand. Sensory satisfaction in these regions is defined by dynamic realism, where greater interaction and richer feedback enhances user presence and engagement [16]. Likewise, the additional haptic sensory channel offers denser information transfer, enriching tangible interactions and enhancing human–machine communication [45]. By incorporating expressive thermal feedback through nonrestrictive interfaces in these high interaction zones (see "Thermic Exoframe" and "Sensory Sleeve" in Figure 18), designers can unlock impactful experiences in social experiences and accessible communication.

6 Study 3: Torso, Legs, and Feet

6.1 Motivation

The torso, legs, and feet are critical regions for creating immersive XR experiences, particularly in applications involving full-body movement such as sports, training, and rehabilitation. These regions are innervated by the sacral and coccygeal plexuses, which cover broad and functionally important surfaces of the body. This study aimed to map the effective sites and perceptual spread of thermal masking across posture- and movement-related body areas. We systematically evaluated three anatomical regions: torso, legs, and feet.

6.2 Participants

Twelve individuals (all males; $M = 25.1$, $SD = 5.1$, $Min = 19$, $Max = 34$; all right-handed) participated in this study. None overlapped with participants from previous studies. Participants underwent the same screening procedure as in the previous study. Recruitment followed the same procedure as Study 1.

6.3 Study Design

A within-subjects design was used to map the perceptual characteristics of thermal masking across the torso, legs, and feet. All trials were conducted on the left side of the body, using bilateral symmetry to limit session length. Stimulation sites were chosen for their alignment with major cutaneous nerve pathways and practical relevance for haptic suit and clothing-based XR interfaces. Depending on the region, the small hardware setup was used for the feet, and the large setup was used for the torso and legs (see Section 3). The torso region is characterized by expansive, predominantly planar surfaces on both the anterior and posterior sides. We utilized large module capable of covering significant surface areas. Anatomically, we differentiated between the ventral and dorsal surfaces to account for varying interaction areas. This arrangement also considered the XR suit, with the high-encounter, torso-focused scenarios such as shooting games and firefighter simulation. The lower limb presents a cylindrical geometry similar to the arm, but with a greater surface area distributed across the thigh and lower leg. Accordingly, we employed the large module setup for this region. Stimulus sites were distributed to cover the length of the limb, prioritizing the large muscle groups of the quadriceps and the tibialis anterior. We also considered the practical constraints of XR hardware, specifically aligning our sites with the interaction zones of exercising or rehabilitation training. The foot involves complex, high-curvature surfaces with a distinct functional separation between the weight-bearing plantar side and the dorsal side. To accommodate this, we implemented the small module. Site selection focused on the toes and metatarsus, regions critical for balance and movement. Furthermore, we considered the affordances of haptic shoes and insoles, targeting areas where embedded actuators typically interface with

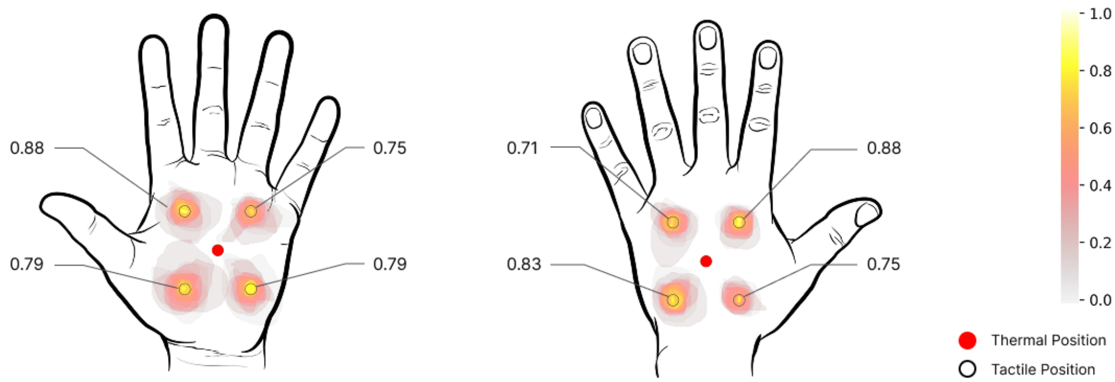

Figure 10: Distribution of perceived thermal illusion of Hand conditions with occurrence rate noted for each tactile position.

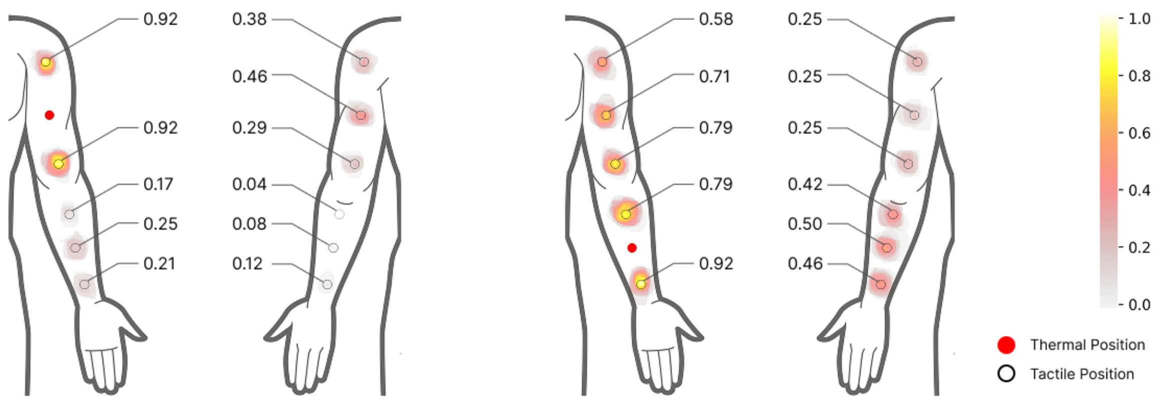

Figure 11: Distribution of perceived thermal illusion of Arm conditions with occurrence rate noted for each tactile position.

the foot. As with previous sections, the precise locations were finalized following pilot tests to confirm effective stimulus transmission for all regions.

- **Torso region:** The ventral and dorsal surfaces were tested separately. Each surface was divided into a 5×2 grid spanning shoulder to hip. From this grid, six sites were selected for thermal stimulation (rows 1, 3, and 5). Each thermal site was paired with all tactile sites, yielding 108 conditions (see Figure 13 (a)).
- **Leg region:** Twelve positions were distributed evenly across the thigh and lower leg. Two ventral sites (center of thigh and center of lower leg) were thermal sites, resulting in 22 conditions (Figure 13 (b)).
- **Feet region:** The plantar and dorsal surfaces were tested separately. Each surface had five positions: one central site and four forming a 2×2 grid near the toes and metatarsus. The central site on each surface served as the thermal site, yielding 8 conditions (Figure 13 (c)).

Measures. As in Studies 1 and 2, occurrence rates of thermal masking and drawn distributions of perceived areas were collected.

6.4 Procedure

The procedure followed Studies 1 and 2. Participants stabilized skin temperature before trials, and each trial delivered simultaneous thermal and tactile stimulation for 5 seconds. The large setup was used for torso and legs, and the small setup for feet.

6.5 Results

Overall Observations. Across torso, legs, and feet, thermal masking was generally clustered around the stimulation site (see Figures. 14-17). On larger surfaces, referral patterns were shaped by both somatotopic proximity and nerve distributions. Same power analysis was conducted as the previous study to validate the sample size and repetition. The reliability result of ICC(2,k) yield a moderate score of 0.67 for 2 repetitions.

Torso. Referred sensations on the torso were clustered but also extended beyond the immediate site, particularly in the lower torso (both the ventral and dorsal surfaces, see Figures. 14-15). The perceived area of sensation was often substantially larger than the

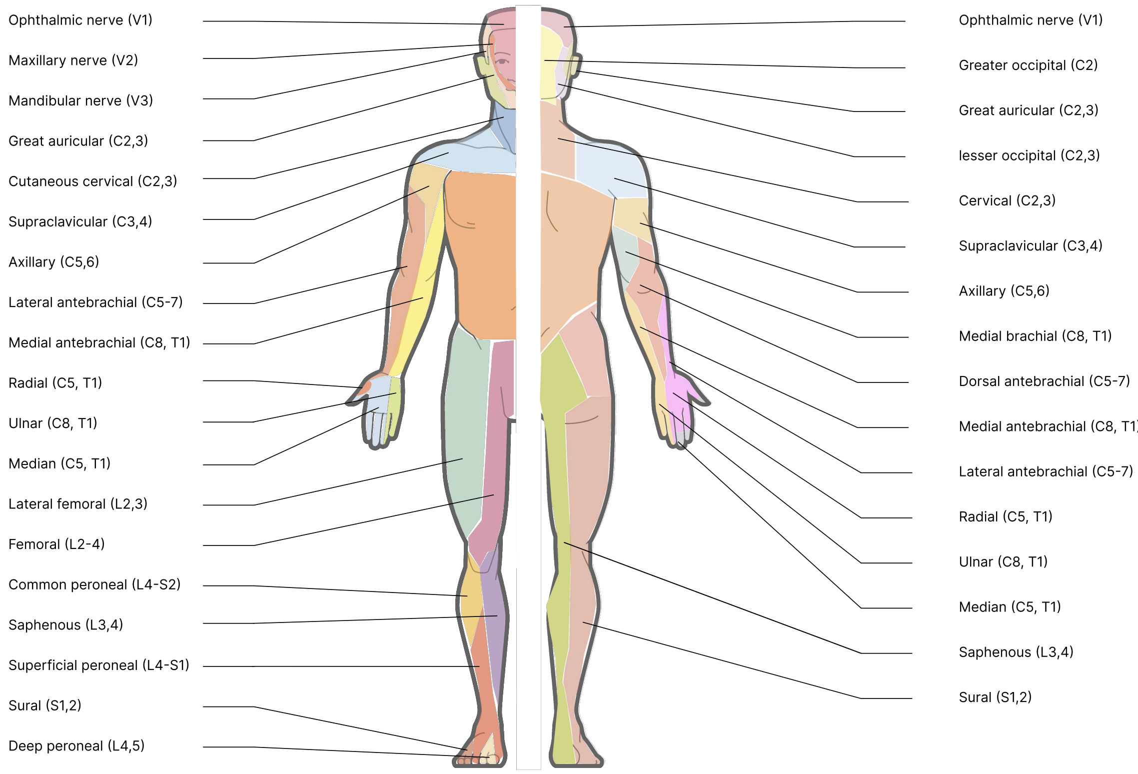

Figure 12: Cutaneous distribution of peripheral nerves.

physical stimulus, sometimes encompassing multiple adjacent tactile sites (e.g., when stimulating at Torso 5 and Torso 20), which indicates a significant spatial spread of the illusion.

Statistical analysis confirmed these observations. On the ventral torso, a two-way RM-ANOVA showed significant effects of thermal position ($F(5, 55) = 5.69$, $p < .01$, $\eta_p^2 = .072$), tactile position ($F(9, 99) = 9.33$, $p < .01$, $\eta_p^2 = .062$), and their interaction ($F(45, 495) = 27.69$, $p < .01$, $\eta_p^2 = .25$). Post-hoc comparisons identified Torso 5, 6, 9, and 10 as optimal sites ($p < .01$), with high occurrence rates (> 75%) in clusters such as Torso 6–7 and Torso 7–10 (see Figure 14).

On the dorsal torso, similar results emerged, with significant effects of thermal ($F(5, 55) = 5.51$, $p < 0.01$, $\eta_p^2 = 0.069$), tactile ($F(9, 99) = 9.33$, $p < .01$, $\eta_p^2 = .079$), and their interaction ($F(45, 495) = 27.69$, $p < .01$, $\eta_p^2 = .29$). Optimal sites included Torso 15, 16, 19, and 20, producing clustered referrals above 80% (see Figure 15).

Leg. On the leg, referral was more localized but sometimes extended across medial–lateral boundaries (see Figure 16). The illusion also showed moderate referral to the contralateral side of the limb.

A two-way RM-ANOVA revealed significant effects of tactile position ($F(11, 121) = 45.7$, $p < 0.01$, $\eta_p^2 = 0.39$) and thermal × tactile interaction ($F(11, 121) = 45.7$, $p < .01$, $\eta_p^2 = .39$). Post-hoc comparisons confirmed localized clusters: for Leg 2, strongest referral was to Leg 1 and 3; for Leg 5, strongest referral was to Leg 4 and 6 (both > 80%).

Feet. Referral on the feet was highly uniform across both plantar and dorsal surfaces (see Figure 17). The perceived area was widespread but consistently centered around reported tactile sites. Statistical analysis confirmed no significant differences by tactile position, consistent with uniform distributions.

Cross-region comparison. Each region showed distinct spatial patterns. On the torso, referral clustered around selective sites with both lateral and vertical spread. On the leg, referral was localized but symmetrical across the limb. The feet showed uniformly high referral across tested sites, unlike the hand in Study 2, where central palm stimulation dominated.

Additional observations.

- On the torso, vertical spread was comparable to lateral spread, suggesting somatotopic proximity may outweigh lateral nerve distributions. For example, stimuli at Torso 5 strongly referred to both lateral (Torso 6) and vertical (Torso 7) sites.
- On the feet, nearly all sites showed high occurrence rates (> 70%), except Foot 5, which lies near the anatomical boundary between the sural and deep peroneal nerves.

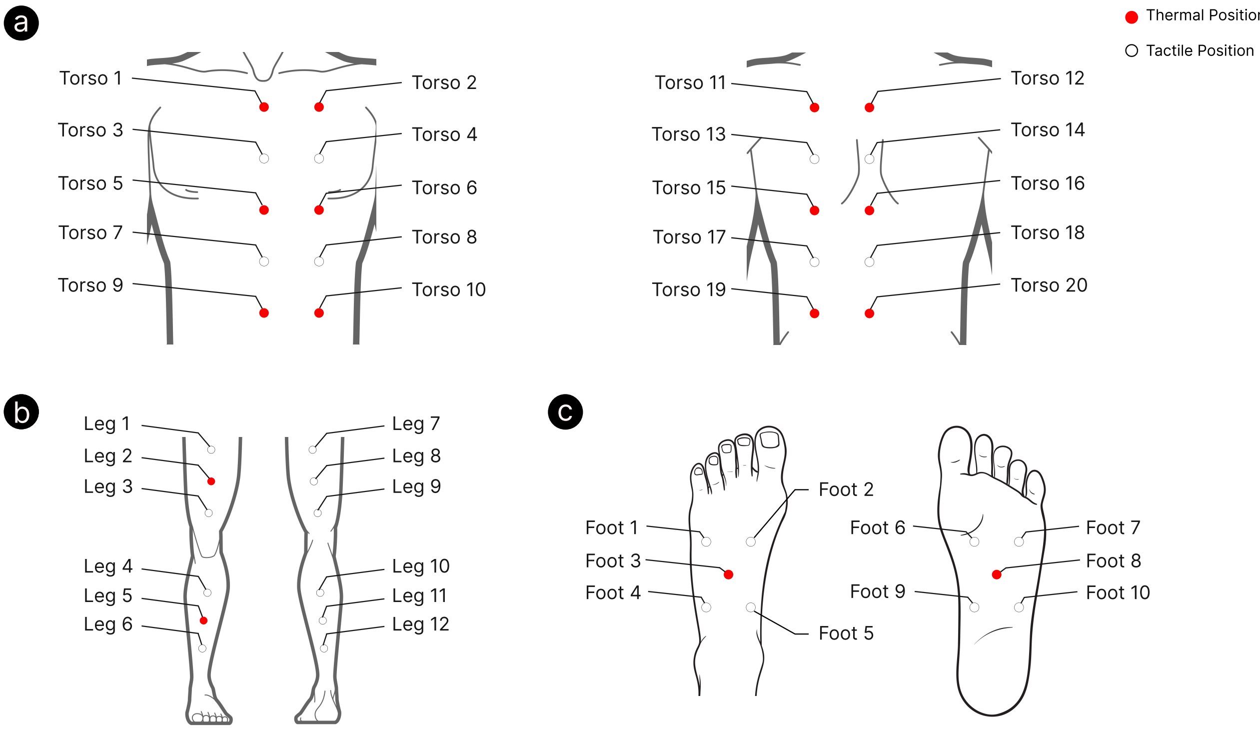

Figure 13: Tested positions for (a) Torso, (b) Leg, and (c) Feet. The red circle indicates the positions for thermal stimuli. The black circle indicates the positions for tactile stimuli other than the thermal position.

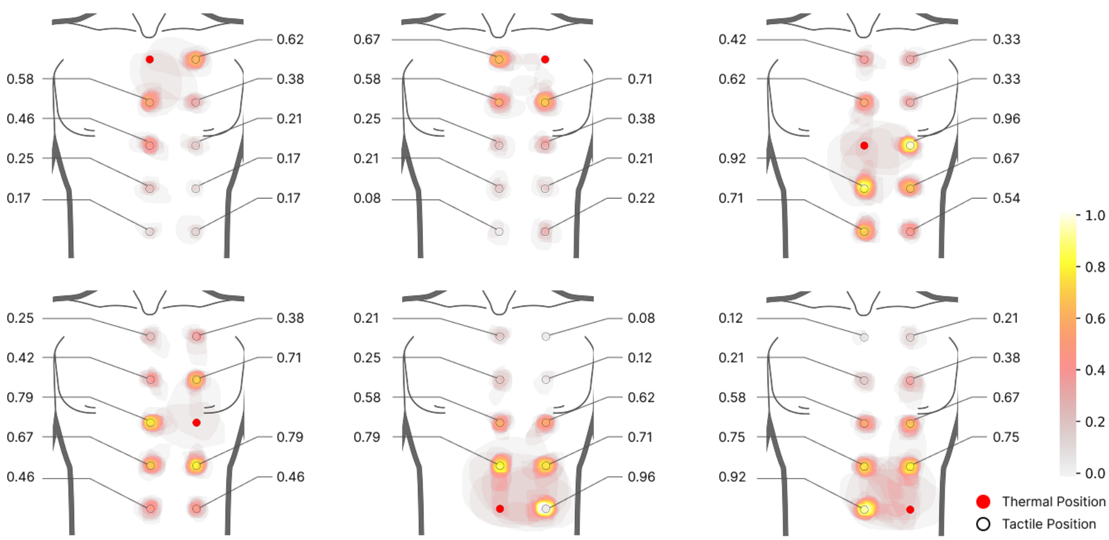

Figure 14: Distribution of perceived thermal illusion of Torso ventral conditions with occurrence rate noted for each tactile position.

6.6 Discussion

Study 3 demonstrated region-specific differences in thermal masking across the torso, legs, and feet.

On the torso, referral clustered around effective thermal sites but extended in both lateral and vertical directions, despite lateralized nerve distributions (see Table 1). Strong correlations between referral rate and vertical distance (ventral $r(24) = -0.87, p < .01$; dorsal

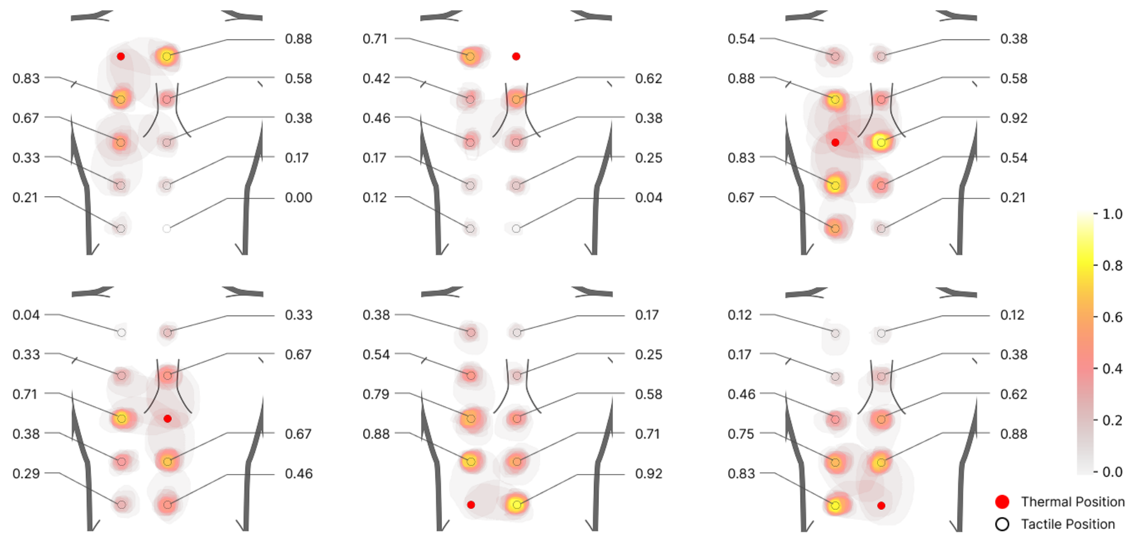

Figure 15: Distribution of perceived thermal illusion of Torso dorsal conditions with occurrence rate noted for each tactile position.

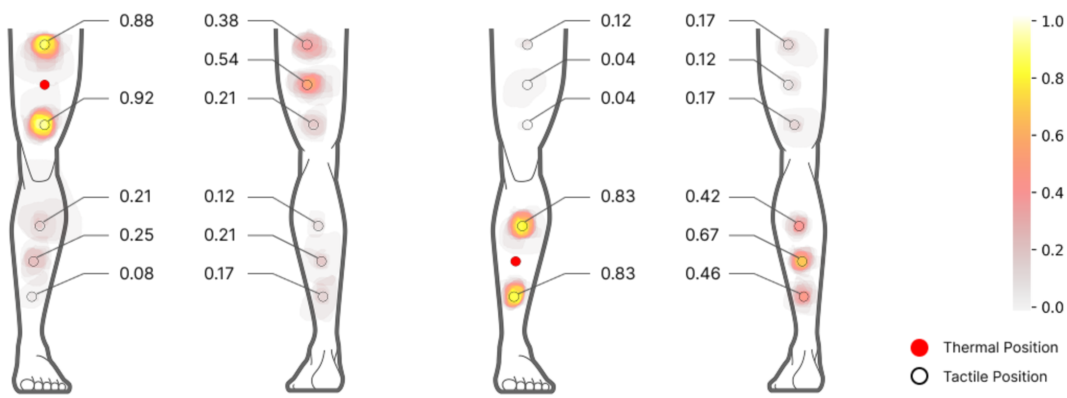

Figure 16: Distribution of perceived thermal illusion of Leg conditions with occurrence rate noted for each tactile position.

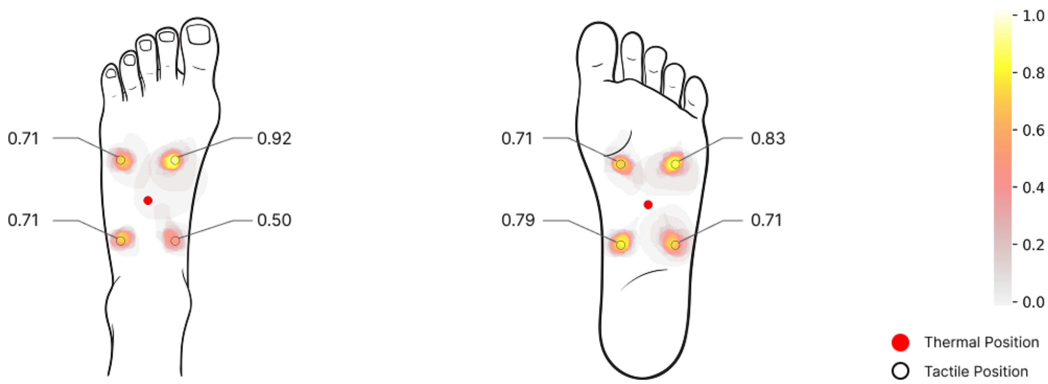

Figure 17: Distribution of perceived thermal illusion of Feet conditions with occurrence rate noted for each tactile position.

Table 1: Occurrence rates on the torso region comparing the lateral and vertical axes.

Torso Ventral						
Tactile	Thermal Position					
Position	torso1	torso2	torso5	torso6	torso9	torso10
Lateral	0.67 (±0.39)	0.61 (±0.47)	0.96 (±0.14)	0.96 (±0.14)	0.91 (±0.19)	0.92 (±0.19)
Vertical1	0.58 (±0.47)	0.71 (±0.45)	0.46 (±0.45)	0.38 (±0.38)	0.17 (±0.25)	0.33 (±0.39)
Vertical2	0.46 (±0.45)	0.38 (±0.38)	0.63 (±0.38)	0.71 (±0.41)	0.25 (±0.39)	0.38 (±0.43)
Vertical3	0.25 (±0.34)	0.21 (±0.26)	0.92 (±0.29)	0.79 (±0.39)	0.71 (±0.45)	0.67 (±0.44)
Vertical4	0.17 (±0.25)	0.21 (±0.33)	0.71 (±0.45)	0.67 (±0.44)	0.79 (±0.33)	0.75 (±0.34)

Torso Dorsal						
Tactile	Thermal Position					
Position	torso11	torso12	torso15	torso16	torso19	torso20
Lateral	0.75 (±0.34)	0.83 (±0.33)	0.96 (±0.14)	0.96 (±0.14)	0.96 (±0.14)	0.96 (±0.14)
Vertical1	0.67 (±0.39)	0.79 (±0.33)	0.58 (±0.47)	0.50 (±0.47)	0.08 (±0.29)	0.08 (±0.29)
Vertical2	0.58 (±0.47)	0.5 (±0.47)	0.71 (±0.45)	0.71 (±0.4)	0.33 (±0.44)	0.25 (±0.4)
Vertical3	0.29 (±0.43)	0.29 (±0.43)	0.88 (±0.23)	0.92 (±0.29)	0.71 (±0.45)	0.62 (±0.43)
Vertical4	0.08 (±0.29)	0.08 (±0.29)	0.71 (±0.45)	0.62 (±0.43)	0.91 (±0.19)	0.79 (±0.33)

$r(24) = -0.86, p < .01$) indicate that proximity strongly influences spread along the vertical axis.

On the leg, referral was localized but symmetric between upper and lower portions of the limb. The illusion was strongest near the thermal site, with moderate contralateral spread, consistent with the broad lateral innervation of the leg.

On the feet, referral was uniformly strong but concentrated, showing less dispersion compared to the hand. This suggests higher thermal acuity and stricter localization, possibly reflecting differences in sensory integration between distal extremities.

Design Implications. For torso-based XR suits, actuator density must be relatively high, particularly across both ventral and dorsal surfaces, to ensure coverage of clustered but selective referral sites. On the legs, efficient coverage can be achieved by targeting upper and lower limb centers, leveraging symmetrical spread while supplementing with additional sites to capture contralateral effects. On the feet, high-density placement is necessary, as masking is highly localized and does not naturally spread to distant sites; footwear interfaces will require more actuators to achieve full coverage. Overall, these results suggest that torso and leg coverage can be achieved with strategic but clustered actuator placement, whereas foot coverage requires dense arrays given its high acuity and limited spread.

In Application. The central and lower body regions benefit from conventional, well-conforming wearables that make thermal feedback integration straightforward. The haptic vest is a common approach to immersive technology [35], and everyday clothing like shoes, pants, and leg wraps provide natural, discrete sites for integrating sensory hardware (see "Haptic Footwear" and "Rehab Wrap" in Figure 18). With the wide thermal masking coverage from minimal thermal actuators demonstrated in this study, users can receive expansive sensory feedback without visible hardware bulk. Leveraging standard wearable form factors in this way maintains social acceptability to the new technology. Additionally, while thermal perception in these body regions may exhibit less dynamism and nuance relative to the hands and face, their role in shaping thermal comfort is significant nonetheless [6, 10]. The torso, leg, and foot offer alternative rendering channels for more ambient and introspective feedback, enabling affective impacts in meditation, rehabilitation, and mobile interactions.

7 Study 4: Inter-Body & Opposite-Side Masking

7.1 Motivation

Studies 1–3 showed that thermal masking occurs across many body regions, with distinct patterns shaped by proximity and peripheral nerve distributions. Building on this, we examined whether referral can extend across anatomical boundaries—either between contiguous body regions (inter-body) or across the midline to contralateral sites (opposite-side). Understanding these extended effects is important for expanding the design space of thermal illusions in XR suits and full-body haptic systems.

7.2 Participants

Twelve individuals (all males; $M = 23.9$, $SD = 3.5$, $Min = 20$, $Max = 32$; all right-handed) participated in this study. Recruitment followed the same procedure as in previous studies, and none overlapped with earlier participants. Participants underwent the same screening procedure as in the previous study.

7.3 Study Design

A within-subjects design was used to map the perceptual characteristics of thermal masking under inter-body and opposite-side conditions. Inter-body stimulations were defined to maintain haptic continuity across anatomically adjacent regions. Optimal stimulation sites identified in prior work were incorporated, with priority given to “nearest-neighbor” coverage—for example, ensuring seamless transitions between individual fingers. Additional sites were selected based on kinematic compatibility with typical XR interface usage, linking body regions that exhibit functional coupling during common movements (e.g., coordination between the torso and limbs during running) to support realistic full-body motion feedback. Opposite-side pairings were deliberately included to enable volumetric XR effects while satisfying ergonomic constraints. In particular, dorsal–ventral configurations were chosen to reproduce “through-body” sensations (e.g., simulated projectile penetration or pass-through effects). The use of thermal actuators on dorsal surfaces was further motivated by the potential to reduce the number of actuators required while preserving comfort and freedom of movement—such as allowing unobstructed ventral hand grasping when wearing an XR glove. Pilot testing for site selection was conducted following the same procedures as in previous studies.

- **Inter-body conditions:** We tested seven contiguous region pairs: Head–Face, Face–Neck, Hand–Finger, Hand–Arm, Torso–Arm, Torso–Leg, and Leg–Foot. For each, the nearest sites were selected as thermal and tactile stimulation points.
- **Opposite-side conditions:** We tested symmetric thermal–tactile pairs across the midline for three regions not previously examined: Hands, Torso, and Feet.

Table 2: Interbody and Opposite Side Occurrence Rates. V indicates ventral and D indicates dorsal.

Inter-Body	Average Occurrence Rate	
	Thermal-Tactile	Tactile-Thermal
Head - Face	0%	0%
Face - Neck	25%	45.8%
Palm - Thumb	33.3%	20.8%
Palm - Index	25%	12.5%
Palm - Middle	43.1%	12.5%
Palm - Ring	45.8%	20.8%
Palm - Pinky	50%	36.1%
Hand - Thumb	16.7%	33.3%
Hand - Index	25%	25%
Hand - Middle	29.2%	16.7%
Hand - Ring	16.7%	29.2%
Hand - Pinky	33.3%	29.2%
Neck - Torso	0%	0%
Neck - Back	0%	0%
Palm - Arm	0%	4.2%
Hand - Arm	8.3%	4.2%
Torso - Arm	54.2%	16.7%
Back - Arm	29.2%	25%
Torso - Leg	4.2%	12.5%
Back - Leg	8.3%	12.5%
Leg - Feet	0%	0%
Leg - Sole	0%	0%

Opposite-Side	Average Occurrence Rate	
	Thermal-Tactile	Tactile-Thermal
Thumb (V) - Thumb (D)	80.5%	79.2%
Index (V) - Index (D)	83.3%	91.7%
Middle (V) -Middle (D)	83.3%	75%
Ring (V) - Ring (D)	95.8%	83.3%
Pinky (V) - Pinky (D)	83.3%	91.7%
Palm (V) - Hand (D)	20.8%	12.5%
Torso1 (V) - Torso12 (D)	12.5%	25%
Torso2 (V) - Torso11 (D)	12.5%	25%
Torso5 (V) - Torso16 (D)	37.5%	72.2%
Torso6 (V) - Torso15 (D)	25%	56.9%
Torso9 (V) - Torso20 (D)	16.7%	70.8%
Torso10 (V) - Torso19 (D)	37.5%	58.3%
Sole (V) - Feet (D)	8.3%	0%

Measures. Occurrence rates of thermal masking and drawn distributions of perceived areas were collected, consistent with Studies 1-3.

7.4 Procedure

The procedure followed previous studies. The large setup was used for Torso, Arm, and Leg trials, and the small setup for Head, Face, Neck, Hand, and Feet trials.

7.5 Results

Overall Observations. Thermal masking across extended regions was highly selective and non-uniform (see Table 2). Opposite-side effects were strongest in fingers, while feet showed minimal masking. Inter-body effects were weaker overall, but clear patterns emerged based on proximity and neuroanatomical continuity. Same power analysis was conducted as the previous study to validate the sample size and repetition. The reliability result of ICC(2,k) yield a moderate score of 0.63 for 2 repetitions.

Inter-body. In most cases, inter-body masking did not occur, underscoring the difficulty of inducing referral across major anatomical boundaries. Pairings such as Head–Face, Neck–Torso, and Leg–Feet yielded almost no reports of illusions, suggesting that strong separation in both innervation and physical distance prevents effective transfer.

That said, a few neighboring regions showed occasional referral when they shared partial nerve pathways and were in close proximity. For example, some participants reported moderate effects in Face–Neck, Palm–Finger, Hand–Finger, and Torso–Arm pairings. Among these, Torso–Arm produced the strongest effects, with an average occurrence of 54.2% when the thermal stimulus was applied to the torso.

Interestingly, these referrals were often asymmetric. Swapping the thermal and tactile sites produced markedly different results, indicating that the direction of stimulation matters. In the Torso–Arm case, referral dropped sharply to 16.7% when the thermal site was placed on the arm. A GLMM analysis confirmed this asymmetry ($\beta = -0.06, p < .01$), highlighting that inter-body masking is not only rare but also directionally selective.

Opposite-side. Masking across the body's midline was strongly dependent on the region, with some areas showing robust bilateral integration and others showing little or none. The fingers produced the clearest effect: masking occurred consistently across all digits, with overall rates above 75% and the index, ring, and pinky exceeding 90%. This aligns with the high tactile acuity and symmetrical innervation of the hands, making them especially receptive to cross-side masking.

The torso also showed reliable but more selective patterns. Masking was concentrated in the lower torso, mirroring within-side results from Study 3. GLMM analysis confirmed significant effects at paired sites such as Torso 5/16 ($\beta = 0.29, p < .01$). Notably, a directional bias emerged: masking was stronger when the thermal site was on the dorsal side (72.2%) than when placed on the ventral side (37.5%).

By contrast, the hands (palm vs. dorsum) and feet exhibited minimal opposite-side masking, generally below 20%. These effects were weaker still when the thermal stimulus originated from dorsal sites. Together, these results suggest that opposite-side masking is strongest in regions with fine bilateral integration (fingers), moderate in regions with structured vertical organization (torso), and weakest in distal extremities such as the feet.

7.6 Discussion

Study 4 revealed that inter-body and opposite-side masking were highly selective and generally weaker than within-region effects. Masking rarely crossed major anatomical boundaries, even when the individual regions involved (such as fingers or palms) were otherwise highly responsive. This suggests that thermal masking is primarily mediated within contiguous nerve branches and does not easily propagate across separate innervation fields.

A consistent asymmetry was also observed. For example, masking from torso to arm was substantially stronger than the reverse, highlighting a directional preference in cross-region effects. Such asymmetry suggests that placement of thermal actuators should consider both location and optimal direction of induced masking.

For opposite-side masking, clear regional differences emerged. The fingers exhibited strong bilateral masking ($> 75\%$), consistent with their symmetrical innervation and high tactile acuity. The torso showed moderate and selective masking, strongest in the lower torso and with a preference for dorsal stimulation. In contrast, the feet showed very weak cross-side masking ($< 20\%$), indicating limited bilateral integration in distal extremities.

Design implications. These findings highlight several strategies for XR haptic system design. Since inter-body masking was often asymmetrical, actuator placement should prioritize directions that yield stronger effects, such as torso-to-arm rather than the reverse, ensuring efficient coverage. On the fingers, bilateral effects can be leveraged by placing actuators dorsally, which allows masking to occur on both sides and frees the ventral surfaces for interaction with virtual objects. On the torso, localized masking patterns suggest that lower and dorsal sites are especially effective, but they cannot substitute for ventral coverage of the upper torso, which requires additional stimulation sites. Finally, understanding these asymmetrical and bilateral patterns enables the creation of dynamic, sequenced effects—for instance, pairing foot stimulation with torso-induced masking to simulate the sensation of a ball's impact traveling upward through the body.

In Application. Ultimately, these inter-body insights highlight the significance of full-body integration for immersive feedback. Thermal coverage in truly immersive applications is guided not only by regional constraints but rather global characteristics [22, 36]. Enhancing expression by these principles shows promise for more realistic simulations, such as hot directional cues in firefighting training, and globally dynamic sensations, like cool water running down the body during a shower. By realizing cost-efficient and lightweight full-body systems, designers are enabled to convey thermally-rich environments with nuance and dynamism.

8 General Discussion

Across four studies, we found that thermal masking follows systematic patterns shaped by both neural innervation and spatial proximity rather than occurring uniformly across the body. High-acuity regions such as the fingers and face produced localized and reliable masking, whereas larger areas like the torso and legs yielded broader but weaker effects. Illusions were generally more effective within single nerve branches than across boundaries, though proximity sometimes overrode neural separations. Extended conditions further highlighted these constraints: inter-body masking was largely ineffective, while opposite-side masking was robust in the fingers but weak in larger, low-sensitivity regions. Together, these findings provide a unified view of how neuroanatomical structure and regional sensitivity govern thermal masking, offering a foundation for XR interface design and theoretical insights into somatosensory integration.

8.1 Cross-Study Synthesis

When compared across all tested regions, several unifying patterns of thermal masking become evident, highlighting the interplay of neural pathways, body sensitivity, and anatomical boundaries.

First, nerve pathways consistently shaped masking strength and spread. Supraorbital stimulation on the face (ophthalmic branch, V1) produced strong masking to adjacent V1 sites but weak effects on nearby V2 sites, despite their closer physical proximity. Similar effects appeared on the hand, where masking was stronger within the digital–ulnar territory than between median and ulnar nerves. On the torso and legs, dermatomal alignment influenced whether sensations spread laterally or vertically, with vertical spread showing strong inverse correlations with distance. These observations align with prior reports that referral is constrained by nerve field continuity rather than pure geometric proximity [42].

Second, regional thermal sensitivity determined perceptual area. High-sensitivity, small regions such as the fingers and head generated tightly localized, high-intensity masking, while lower-sensitivity, larger regions such as the torso and arm produced more dispersed areas of referral. Intermediate regions, including the palm, neck, and feet, supported broader but stable coverage, suggesting a balance between precision and spread. These differences are consistent with the known variance in thermal sensitivity across the body [21], and parallel earlier findings of localized illusions in the fingers [41] versus more distributed spread on the torso [35] and arm [42].

Third, cross-boundary effects were limited and asymmetric. Inter-body masking was generally ineffective across major anatomical divides, but some exceptions emerged where proximity and shared pathways aligned—for example, between the torso and arm, or between palm and finger. Opposite-side masking was robust for fingers, supporting bilateral integration, but sparse for torso and feet. Importantly, these effects were not always reciprocal: torso-to-arm transfer was stronger than arm-to-torso, and dorsal torso stimulation induced more reliable opposite-side masking than ventral stimulation. Such asymmetry suggests that extended referral may be mediated by directional neural connectivity rather than symmetric cross-hemispheric integration.

These results establish three governing principles: masking is strongest within nerve branches, proximity can partially override anatomical boundaries, and asymmetry emerges in both inter-body and bilateral contexts. This framework unifies local and extended masking phenomena across the body while situating them within prior evidence of regional sensitivity and somatotopic mapping.

8.2 Principles for XR Thermal-Tactile Interface Design

Our results across all four studies highlight several general principles for designing XR interfaces that leverage thermal–tactile masking. These guidelines translate the perceptual findings into actionable strategies for maximizing coverage, reducing hardware cost, and aligning actuator placement with neuroanatomical constraints (see Figure 1).

A consistent observation across participants was that the referred thermal sensation often dominated the physical thermal source. Participants described the thermal site as "less noticeable," "secondary," or "fading," while the referred location produced the vivid percept. This salience hierarchy has strong design implications: thermal actuators do not need to be co-located with the point of interaction. Designers can place bulkier thermal modules at proximal sites along a nerve pathway (e.g., forearm, torso), leaving high-mobility regions such as fingers or the face free for light, precise vibrotactile arrays. This division of labor reduces hardware burden while preserving dexterity and interaction fidelity.

Insight 1: Target high-yield regions for efficiency. Masking strength varied by body region. Locations such as the supraorbital ridge, central palm, dorsal torso, and lateral neck consistently produced broad spread, enabling large perceptual coverage with minimal hardware.

In HMDs, placing a thermal module near a supraorbital region can cover much of the upper face. Neck- or collar-based wearables can use lateral sites to deliver wrap-around thermal cues. Gloves or sleeves can place thermal modules at central palm or mid-forearm locations to minimize the number of required thermal elements while still providing rich distal sensations. Thermal modules in vests should be positioned at dorsal and ventral midline areas (e.g., between vertebral segments) to maximize coverage with minimal density. These configurations reduce thermal actuator count while maintaining perceptual realism.

Insight 2: Align actuators with neural pathways. Thermal masking follows cutaneous nerve branches, not simple geometric distance. Illusory spread along median, ulnar, radial, trigeminal, and spinal pathways was stronger than spread in purely nearby skin regions. In HMDs, thermal elements placed along V1/V2/V3 divisions can reach broad peri-orbital, cheek, and jaw areas. Gloves should place thermal modules dorsally along the pathways of the radial and ulnar nerves, leaving palmar surfaces unobstructed. Sleeves should align actuators along median-ulnar-radial territories to extend sensations toward the wrist or elbow. In thermal vests, placement along the spinal column or rib lines aligns with major thermal afferents, enabling broad perceptual coverage.

Designers should confirm coverage through quick perceptual mapping pilots and ensure both within-nerve and cross-nerve referral patterns are achieved.

Insight 3: Adapt actuator density to body regions. Some regions (face, feet) require denser coverage because masking remains localized. Others (torso, palm, forearm) spread readily and can be driven with fewer actuators. High-resolution arrays (1–4 cm spacing) should be reserved for high-acuity regions such as fingers, face, and feet. Low-resolution grids (10–20 cm spacing) are sufficient for broad-area regions such as torso and limbs. Temperature change rates should also adapt to region and garment conditions (≈ 6 °C/s on bare skin; > 10 °C/s through clothing).

Actuator budgets should therefore be region-specific: dense where necessary, sparse where possible. This ensures immersive rendering without unnecessary hardware.

Insight 4: Exploit asymmetry and cross-body effects. Thermal masking is directionally asymmetric (e.g., torso → arm is stronger than arm → torso), and dorsal regions often support broader spread than ventral regions. Place thermal sources on low-interaction, low-mobility areas (e.g., torso, dorsal digits) to evoke sensations in high-interaction areas (e.g., hands, ventral digits) without physically instrumenting them. Use dorsal surfaces for thermal modules and ventral surfaces for manipulation-related vibrotactile cues. For tasks requiring unencumbered hands, thermal modules can be placed proximally (e.g., upper arm, torso), yet still produce vivid distal sensations. This reduces actuator redundancy and improves ergonomics.

Insight 5: Use dynamic sequencing for complex events. Temporal chaining of thermal and vibrotactile cues produces convincing directional motion illusions and event dynamics. For impact events (e.g., a virtual kick), trigger a vibrotactile cue at the distal site and a thermal cue at a proximal site to simulate momentum traveling across the limb. For motor rehabilitation, sequence thermal cues proximally (e.g., elbow→wrist) and vibrotactile cues distally (e.g., fingertips) to guide coordinated reaching. For gait training, use hip→knee→ankle thermal sequencing followed by a vibrotactile "heel-strike" marker to scaffold natural walking rhythms.

Sequencing allows lightweight XR wearables to simulate complex physical dynamics without heavy actuation.

General Principle. Across all regions, the most efficient XR designs: Use high-yield **thermal sites**; align with **nerve pathways**; vary **density** according to region; exploit directional **asymmetry**; Sequence thermal–tactile cues **temporally**. Together, these strategies enable immersive multisensory experiences with few actuators, scaling from gloves to full-body thermal suits.

8.3 Application-Level Design Patterns for XR and Assistive Technologies

Building on the perceptual principles established across Studies 1–4, we outline three application-level design patterns that translate whole-body masking characteristics into concrete design strategies for XR systems, immersive training, telepresence, and assistive technologies. These scenarios expand the human-centered contribution of the work by demonstrating how thermal–tactile illusions can

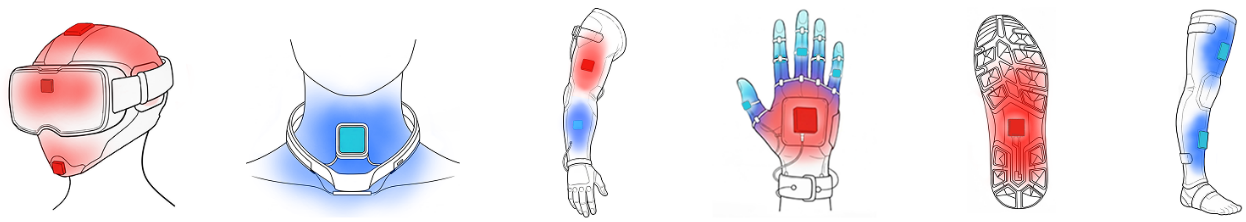

Figure 18: Concept sketches of wearable interfaces show optimal thermal actuator placement, informed by Studies 1–4, enabling efficient thermal masking with minimal thermal actuators and strategically placed vibrotactile actuators. Integrated with conventional wearables, these designs point toward broader accessibility and application of thermal feedback.

improve usability, comfort, affective engagement, and accessibility in real deployments.

Design Scenario A: Minimalist Wearables for Everyday XR Use. Our cross-region analyses demonstrate that masking is highly concentrated at specific high-efficacy sites. On the torso, eight locations produced occurrence rates above 75% and reliably spread to neighboring regions. On the hand, central-palm stimulation consistently covered the entire hand, and only three finger sites—thumb, middle, and pinky—generated near-complete perceptual coverage via within-nerve propagation. These patterns suggest that expressive multisensory feedback does not require dense, uniformly distributed thermal arrays. A minimalist system with roughly twenty-five to thirty actuators placed only at high-yield sites can reproduce the perceptual coverage of traditional sixty-plus actuator configurations (see "Thermal HMD" and "Thermic Exoframe" in Figure 18). This reduction yields significant human-centered benefits: devices become lighter, cooler, and less obtrusive; battery life improves; mechanical pressure on the skin is reduced; and long-duration use becomes more comfortable. Such systems are especially well suited for daily XR productivity, collaborative environments, industrial or medical training sessions, and other scenarios of extended wear without compromising mobility or comfort.

Design Scenario B: Immersive VR, Gaming, and Telepresence through Dynamic Sequencing. Study 4 revealed robust directional asymmetries—for instance, torso-to-arm transfer was more than three times stronger than arm-to-torso—and Studies 2 and 3 showed that the hands exhibit strong bilateral masking. These findings open new possibilities for dynamic cue sequencing that enhances presence, emotional engagement, and motor coordination. A virtual handshake, for example, can be rendered by stimulating dorsal finger sites and then progressing the combined thermal–tactile sensation proximally toward the wrist, mirroring the natural temporal pattern of interpersonal touch. Impact-based events such as sports collisions or object interactions can similarly be conveyed by initiating a vibrotactile pulse at the foot and chaining a thermal illusion toward the torso and arms, producing a coherent sense of energy transfer (see "Haptic Footwear" and "Sensory Sleeve" in Figure 18). These effects extend beyond entertainment: in collaborative VR or social telepresence, sequences of warm and tactile cues can reinforce shared attention, turn-taking, or interpersonal gestures. Dynamic sequencing—guided by the body's natural connectivity patterns—enables a level of perceptual expressiveness that would be impractical with static actuator placement alone, making immersive XR more engaging and emotionally resonant.

Design Scenario C: Assistive and Rehabilitative Technologies. The high-confidence perceptual channels revealed across all studies, particularly the >80% occurrence rates on the hands and fingers and the strong bilateral referral effects, provide a foundation for assistive and rehabilitative interface design. For users with reduced or altered somatosensation—such as stroke survivors, individuals with peripheral neuropathy, or those with spinal cord injury—these high-yield regions offer reliable perceptual anchors for guiding movement, attention, and proprioception. Because masking at the fingers is both robust and bilateral, actuators placed on one hand can create symmetric percepts across both, supporting bimanual coordination training without requiring redundant hardware. Thermal cues on the neck, torso, or leg can also serve as proximal indicators that scaffold timing and movement initiation for rehabilitation exercises, while vibrotactile cues at distal sites mark goal achievement or task completion (see "Rehab Wrap" and "Meditative Necklace" in Figure 18). These capabilities allow designers to tailor feedback strategies to each user's residual sensory abilities, supporting personalized rehabilitation protocols and improving accessibility. Masking thus becomes a mechanism for amplifying sensory feedback in individuals who may not reliably perceive localized thermal or tactile cues.

These scenarios demonstrate that thermal–tactile masking is not merely a perceptual phenomenon but a practical design resource. By strategically leveraging high-efficacy sites, exploiting directional and bilateral referral patterns, and sequencing cues over time, XR systems can achieve rich multisensory experiences with minimal hardware. These design patterns offer pathways toward lighter, more ergonomic, more expressive, and more inclusive XR interfaces—from everyday productivity tools to immersive simulations and rehabilitative technologies.

8.4 Neurophysiological Insights

The present findings raise important questions about the neural mechanisms underlying thermal masking, which remain far from fully understood. Several possible explanations can be drawn. One interpretation is that masking reflects the interaction between coarse thermal maps and finer-grained tactile maps. The strong vertical gradients observed on the torso and the asymmetry in torso-to-arm versus arm-to-torso masking suggest that vibration may constrain or redirect diffuse thermal input, sharpening its perceptual boundaries and relocating its felt position. A related account is the perceptual filling-in hypothesis: prior work on thermal referral indicates that warmth can spread uniformly across unstimulated sites, likely through symbolic completion or propagation in somatosensory cortex [3, 17, 29]. In contrast, masking appears to disrupt this process, as tactile dominance prevents the spread and anchors perception at the vibration site.

Another possible explanation lies in the characteristics of thermal channels themselves. Warm afferents are known to have large receptive fields and exhibit strong spatial summation, which can blur localized signals [2, 38]. Masking may occur when high-resolution tactile input overrides this coarse integration, creating a sharper but relocated percept. Finally, attentional capture may also play a role: vibrotactile input is highly salient and may act as a bottom-up "circuit breaker" [4], reflexively diverting attentional resources to the vibration site and suppressing awareness of concurrent thermal stimulation elsewhere, aligning with the vibration-driven dominance found in our experiments.

8.5 Limitations and Future Work

Several limitations remain and point to promising directions for future work. Individual variability in thermal sensitivity was not explicitly modeled, and a fixed warm stimulus was used to ensure consistent and reliable illusion induction across participants. While this choice supported controlled comparisons across body regions, future studies could explore individualized calibration to further optimize masking strength. Cooling and other temperature ranges were not tested, which may limit generalizability beyond warm stimuli.

Motor vibration stimuli were applied along different axes for the small and large actuators; although the strap-based attachment ensured effective perpendicular transmission of vibration to the skin, this setup limited systematic isolation of force-direction effects. Future work could explicitly examine how vibration axis influences masking strength. Extended-body conditions were sampled at select sites to probe cross-region and bilateral effects, leaving open how masking generalizes across more complex inter-limb and midline configurations.

The assessment of the thermal illusion focused primarily on its spatial characteristics, and the relative perceptual intensity between the physical heat source and the illusory sensation was not directly quantified. Investigating this perceptual balance may provide deeper insight into salience dominance. Temporal dynamics—such as the duration and sequence of stimulation—were not systematically explored, though they may play a crucial role in shaping perceived continuity. Future work should address these aspects by exploring wider temperature ranges, vibration motor oscillation axes, individual calibration, richer inter-body mappings, perceived intensity differences between physical and illusory sensations, and temporal sequencing strategies. Such investigations will further deepen mechanistic understanding of thermal masking and expand its utility in designing next-generation XR haptic systems.

9 Conclusion

Across four studies, we systematically mapped thermal masking across the whole body and identified unifying principles: masking is strongest within nerve branches, modulated by regional thermal sensitivity, and constrained across anatomical boundaries with notable asymmetries. These findings advance the understanding of somatosensory integration and provide concrete strategies for XR design, showing how a few strategically placed actuators can achieve broad perceptual coverage through illusion-driven effects. By treating masking as a resource rather than a limitation, this work lays the foundation for lightweight, efficient, and immersive multisensory interfaces.

Acknowledgments

This work was supported by the NSF Grant 2441833: CAREER: Designing Next-Generation Thermal User Interfaces for Multisensory VR Experiences.

References

[1] Rochelle Ackerley and Roger Holmes Watkins. 2018. Microneurography as a tool to study the function of individual C-fiber afferents in humans: responses from nociceptors, thermoreceptors, and mechanoreceptors. *Journal of Neurophysiology* 120, 6 (2018), 2834–2846. doi:10.1152/jn.00109.2018 PMID: 30256737.

[2] William S Cain. 1973. Spatial discrimination of cutaneous warmth. *The American journal of psychology* (1973), 169–181. doi:10.2307/1421858

[3] Antonio Cataldo, Elisa Raffaella Ferrè, Giuseppe Di Pellegrino, and Patrick Haggard. 2016. Thermal referral: evidence for a thermoceptive uniformity illusion without touch. *Scientific reports* 6, 1 (2016), 1–10. doi:10.1038/srep35286

[4] Maurizio Corbetta and Gordon L Shulman. 2002. Control of goal-directed and stimulus-driven attention in the brain. *Nature reviews neuroscience* 3, 3 (2002), 201–215. doi:10.1038/nrn755

[5] Arthur D Craig and M Catherine Bushnell. 1994. The thermal grill illusion: unmasking the burn of cold pain. *Science* 265, 5169 (1994), 252–255. doi:10.1126/science.8023144

[6] Tamar Dublin and Oren Zuckerman. 2025. The Walking Meditation Mat: Leveraging Targeted Heat Sensation to Guide Attention Inward. In *Proceedings of the 2025 CHI Conference on Human Factors in Computing Systems*. 1–12.

[7] Peter James Dyck, I Zimmerman, DA Gillen, D Johnson, JL Karnes, and PC O'Brien. 1993. Cool, warm, and heat-pain detection thresholds: testing methods and inferences about anatomic distribution of receptors. *Neurology* 43, 8 (1993), 1500–1500. doi:10.1212/WNL.43.8.1500

[8] Abdallah El Ali, Xingyu Yang, Swamy Ananthanarayan, Thomas Röggla, Jack Jansen, Jess Hartcher-O'Brien, Kaspar Jansen, and Pablo Cesar. 2020. ThermalWear: Exploring Wearable On-Chest Thermal Displays to Augment Voice Messages with Affect. In *Proceedings of the 2020 CHI Conference on Human Factors in Computing Systems* (Honolulu, HI, USA) *(CHI '20)*. Association for Computing Machinery, New York, NY, USA, 1–14. doi:10.1145/3313831.3376682

[9] Bettina Eska, Jeff-Owens Iyalekhue, Sebastian Günther, Jasmin Niess, and Florian Müller. 2023. ThermoFeet: Assessing On-Foot Thermal Stimuli for Directional Cues. In *Proceedings of the 22nd International Conference on Mobile and Ubiquitous Multimedia* (Vienna, Austria) *(MUM '23)*. Association for Computing Machinery, New York, NY, USA, 166–171. doi:10.1145/3626705.3627974

[10] Talia Sofia Ezer, Jonathan Giron, Hadas Erel, and Oren Zuckerman. 2024. Somaesthetic Meditation Wearable: Exploring the Effect of Targeted Warmth Technology on Meditators' Experiences. In *Proceedings of the 2024 CHI Conference on Human Factors in Computing Systems*. 1–14.

[11] Davide Filingeri. 2016. Neurophysiology of skin thermal sensations. *Comprehensive Physiology* 6, 3 (2016), 1429–1491.

[12] Haichen Gao, Shaoyu Cai, Yuhong Wu, and Kening Zhu. 2024. ThermOuch: A Wearable Thermo-Haptic Device for Inducing Pain Sensation in Virtual Reality through Thermal Grill Illusion. In *SIGGRAPH Asia 2024 Conference Papers* (Tokyo, Japan) *(SA '24)*. Association for Computing Machinery, New York, NY, USA, Article 138, 12 pages. doi:10.1145/3680528.3687620

[13] Barry G Green. 1978. Referred thermal sensations: warmth versus cold. *Sensory processes* 2, 3 (1978), 220–230.

[14] Sebastian Günther, Florian Müller, Dominik Schön, Omar Elmoghazy, Max Mühlhäuser, and Martin Schmitz. 2020. Therminator: Understanding the Interdependency of Visual and On-Body Thermal Feedback in Virtual Reality. In *Proceedings of the 2020 CHI Conference on Human Factors in Computing Systems*

(Honolulu, HI, USA) *(CHI '20)*. Association for Computing Machinery, New York, NY, USA, 1–14. doi:10.1145/3313831.3376195

[15] Teng Han, Fraser Anderson, Pourang Irani, and Tovi Grossman. 2018. HydroRing: Supporting Mixed Reality Haptics Using Liquid Flow. In *Proceedings of the 31st Annual ACM Symposium on User Interface Software and Technology* (Berlin, Germany) *(UIST '18)*. Association for Computing Machinery, New York, NY, USA, 913–925. doi:10.1145/3242587.3242667

[16] Jeanne Hecquard, Justine Saint-Aubert, Ferran Argelaguet, Claudio Pacchierotti, Anatole Lécuyer, and Marc JM Macé. 2024. Warm regards: Influence of thermal haptic feedback during social interactions in VR. In *2024 IEEE International Symposium on Mixed and Augmented Reality (ISMAR)*. IEEE, 1216–1225.

[17] Hsin-Ni Ho, Junji Watanabe, Hideyuki Ando, and Makio Kashino. 2011. Mechanisms underlying referral of thermal sensations to sites of tactile stimulation. *Journal of Neuroscience* 31, 1 (2011), 208–213. doi:10.1523/JNEUROSCI.2640-10.2011

[18] Daisuke Iwai, Mei Aoki, and Kosuke Sato. 2019. Non-Contact Thermo-Visual Augmentation by IR-RGB Projection. *IEEE Transactions on Visualization and Computer Graphics* 25, 4 (2019), 1707–1716. doi:10.1109/TVCG.2018.2820121

[19] Lynette A Jones and Hsin-Ni Ho. 2025. Tactile–Thermal Interactions: Cooperation and Competition. *IEEE Transactions on Haptics* (2025).

[20] Yuhu Liu, Satoshi Nishikawa, Young ah Seong, Ryuma Niiyama, and Yasuo Kuniyoshi. 2021. ThermoCaress: A Wearable Haptic Device with Illusory Moving Thermal Stimulation. In *Proceedings of the 2021 CHI Conference on Human Factors in Computing Systems* (, Yokohama, Japan,) *(CHI '21)*. Association for Computing Machinery, New York, NY, USA, Article 214, 12 pages. doi:10.1145/3411764.3445777

[21] Maohui Luo, Zhe Wang, Hui Zhang, Edward Arens, Davide Filingeri, Ling Jin, Ali Ghahramani, Wenhua Chen, Yingdong He, and Binghui Si. 2020. High-density thermal sensitivity maps of the human body. *Building and Environment* 167 (2020), 106435. doi:10.1016/j.buildenv.2019.106435

[22] Alex Mazursky, Jas Brooks, Beza Desta, and Pedro Lopes. 2024. ThermalGrasp: Enabling Thermal Feedback even while Grasping and Walking. In *2024 IEEE Conference Virtual Reality and 3D User Interfaces (VR)*. 342–353. doi:10.1109/VR58804.2024.00056

[23] David D. McKemy. 2012. The molecular and cellular basis of cold sensation. *ACS Chem Neurosci* 4 (2012), 238–247. doi:10.1021/cn300193h

[24] Arshad Nasser and Khalad Hasan. 2024. ThermoGrasp: Enabling Localized Thermal Feedback on Fingers for Precision Grasps in Virtual Reality. *Proc. ACM Hum.-Comput. Interact.* 8, MHCI, Article 279 (Sept. 2024), 21 pages. doi:10.1145/3676526

[25] Arshad Nasser, Kexin Zheng, and Kening Zhu. 2021. ThermEarhook: Investigating Spatial Thermal Haptic Feedback on the Auricular Skin Area. In *Proceedings of the 2021 International Conference on Multimodal Interaction* (Montréal, QC, Canada) *(ICMI '21)*. Association for Computing Machinery, New York, NY, USA, 662–672. doi:10.1145/3462244.3479922

[26] Simone Ooms, Minha Lee, Ekaterina R Stepanova, Pablo Cesar, and Abdallah El Ali. 2025. Haptic Biosignals Affect Proxemics Toward Virtual Reality Agents. In *Proceedings of the 2025 CHI Conference on Human Factors in Computing Systems*. 1–18.

[27] Roshan Lalitha Peiris, Yuan-Ling Feng, Liwei Chan, and Kouta Minamizawa. 2019. ThermalBracelet: Exploring Thermal Haptic Feedback Around the Wrist. In *Proceedings of the 2019 CHI Conference on Human Factors in Computing Systems* (Glasgow, Scotland Uk) *(CHI '19)*. Association for Computing Machinery, New York, NY, USA, 1–11. doi:10.1145/3290605.3300400

[28] Roshan Lalintha Peiris, Wei Peng, Zikun Chen, Liwei Chan, and Kouta Minamizawa. 2017. ThermoVR: Exploring Integrated Thermal Haptic Feedback with Head Mounted Displays. In *Proceedings of the 2017 CHI Conference on Human Factors in Computing Systems* (Denver, Colorado, USA) *(CHI '17)*. Association for Computing Machinery, New York, NY, USA, 5452–5456. doi:10.1145/3025453.3025824

[29] Vilayanur S Ramachandran and Richard L Gregory. 1991. Perceptual filling in of artificially induced scotomas in human vision. *Nature* 350, 6320 (1991), 699–702. doi:10.1038/350699a0

[30] Ximing Shen, Youichi Kamiyama, Kouta Minamizawa, and Jun Nishida. 2024. DexteriSync: A Hand Thermal I/O Exoskeleton for Morphing Finger Dexterity Experience. In *Proceedings of the 37th Annual ACM Symposium on User Interface Software and Technology* (Pittsburgh, PA, USA) *(UIST '24)*. Association for Computing Machinery, New York, NY, USA, Article 102, 12 pages. doi:10.1145/3654777.3676422

[31] Yatharth Singhal, Daniel Honrales, and Jin Ryong Kim. 2025. HeatFlow: A Thermal-Tactile Display for Dynamic 2D Thermal Movements. In *Proceedings of the 38th Annual ACM Symposium on User Interface Software and Technology*. 1–18.

[32] Yatharth Singhal, Daniel Honrales, Haokun Wang, and Jin Ryong Kim. 2024. Thermal In Motion: Designing Thermal Flow Illusions with Tactile and Thermal Interaction. In *Proceedings of the 37th Annual ACM Symposium on User Interface Software and Technology* (Pittsburgh, PA, USA) *(UIST '24)*. Association for Computing Machinery, New York, NY, USA, Article 27, 13 pages. doi:10.1145/3654777.3676460

[33] Yatharth Singhal, Haokun Wang, Hyunjae Gil, and Jin Ryong Kim. 2021. Mid-Air Thermo-Tactile Feedback Using Ultrasound Haptic Display. In *Proceedings of the 27th ACM Symposium on Virtual Reality Software and Technology* (Osaka, Japan) *(VRST '21)*. Association for Computing Machinery, New York, NY, USA, Article 28, 11 pages. doi:10.1145/3489849.3489889

[34] Yatharth Singhal, Haokun Wang, and Jin Ryong Kim. 2023. Fire: Mid-air thermo-tactile display. In *SIGGRAPH Asia 2023 Emerging Technologies*. 1–2.

[35] Hyungki Son, Haokun Wang, Yatharth Singhal, and Jin Ryong Kim. 2023. Upper Body Thermal Referral and Tactile Masking for Localized Feedback. *IEEE Transactions on Visualization and Computer Graphics* 29, 5 (2023), 2211–2219. doi:10.1109/TVCG.2023.3247068

[36] Wenjie Song, Fangliang Zhong, John Kaiser Calautit, and Jiaxiang Li. 2025. Exploring the role of skin temperature in thermal sensation and thermal comfort: A comprehensive review. *Energy and Built Environment* 6, 4 (2025), 762–781.

[37] Anelise Sonza, Nina Völkel, Milton A. Zaro, Matilde Achaval, and Ewald M. Hennig. 2015. A whole body vibration perception map and associated acceleration loads at the lower leg, hip and head. *Medical Engineering & Physics* 37, 7 (2015), 642–649. doi:10.1016/j.medengphy.2015.04.003

[38] Joseph C Stevens and Lawrence E Marks. 1971. Spatial summation and the dynamics of warmth sensation. *Perception & Psychophysics* 9, 5 (1971), 391–398. doi:10.3758/BF03210236

[39] Chan Lek Tan and Zachary A Knight. 2018. Regulation of body temperature by the nervous system. *Neuron* 98, 1 (2018), 31–48. doi:10.1016/j.neuron.2018.02.022

[40] Jörg Trojan, Annette M Stolle, Dieter Kleinböhl, Carsten D Mørch, Lars Arendt-Nielsen, and Rupert Hölzl. 2006. The saltation illusion demonstrates integrative processing of spatiotemporal information in thermoceptive and nociceptive networks. *Experimental brain research* 170, 1 (2006), 88–96. doi:10.1007/s00221-005-0190-z

[41] Haokun Wang, Yatharth Singhal, Hyunjae Gil, and Jin Ryong Kim. 2024. Fiery Hands: Designing Thermal Glove through Thermal and Tactile Integration for Virtual Object Manipulation. In *Proceedings of the 37th Annual ACM Symposium on User Interface Software and Technology* (Pittsburgh, PA, USA) *(UIST '24)*. Association for Computing Machinery, New York, NY, USA, Article 101, 15 pages. doi:10.1145/3654777.3676457

[42] Haokun Wang, Yatharth Singhal, Hyunjae Gil, and Jin Ryong Kim. 2024. Thermal Masking: When the Illusion Takes Over the Real. In *Proceedings of the 2024 CHI Conference on Human Factors in Computing Systems* (Honolulu, HI, USA) *(CHI '24)*. Association for Computing Machinery, New York, NY, USA, Article 419, 16 pages. doi:10.1145/3613904.3641941

[43] Haokun Wang, Yatharth Singhal, and Jin Ryong Kim. 2024. Let It Snow: Designing Snowfall Experience in VR. *Proc. ACM Interact. Mob. Wearable Ubiquitous Technol.* 8, 2, Article 54 (may 2024), 24 pages. doi:10.1145/3659587

[44] Alexander Wilberz, Dominik Leschtschow, Christina Trepkowski, Jens Maiero, Ernst Kruijff, and Bernhard Riecke. 2020. FaceHaptics: Robot Arm based Versatile Facial Haptics for Immersive Environments. In *Proceedings of the 2020 CHI Conference on Human Factors in Computing Systems* (Honolulu, HI, USA) *(CHI '20)*. Association for Computing Machinery, New York, NY, USA, 1–14. doi:10.1145/3313831.3376481

[45] Graham Wilson and Stephen A Brewster. 2017. Multi-moji: Combining thermal, vibrotactile & visual stimuli to expand the affective range of feedback. In *Proceedings of the 2017 CHI Conference on Human Factors in Computing Systems*. 1743–1755.

[46] Hyung Ii Yi, Hojeong Lee, and Sang Ho Yoon. 2024. ThermicVib: Enabling Dynamic Thermal Sensation with Multimodal Haptic Glove for Thermal-Responsive Interaction. In *2024 IEEE International Symposium on Mixed and Augmented Reality (ISMAR)*. 614–623. doi:10.1109/ISMAR62088.2024.00076

[47] Hui Zhang. 2003. *Human thermal sensation and comfort in transient and non-uniform thermal environments*. University of California, Berkeley.

[48] Kening Zhu, Simon Perrault, Taizhou Chen, Shaoyu Cai, and Roshan Lalintha Peiris. 2019. A sense of ice and fire: Exploring thermal feedback with multiple thermoelectric-cooling elements on a smart ring. *International Journal of Human-Computer Studies* 130 (2019), 234–247. doi:10.1016/j.ijhcs.2019.07.003